

Smooth Solutions of the tt^* Equation: A Numerical Aided Case Study

Li Yu-Qi

January 2, 2024

Abstract: An important special class of the tt^* equations are the tt^* -Toda equations. Guest et al. have given comprehensive studies on the tt^* -Toda equations in a series of papers. The fine asymptotics for a large class of solutions of a special tt^* -Toda equation, the case 4a in their classification, have been obtained in a paper (Commun. Math. Phys. 374, 923-973) in the series. Most of these formulas are obtained with elaborate reasoning and the calculations involved are lengthy. There are concerns about these formulas if they have not been verified by other methods. The first part of this paper is devoted to the numerical verification of these fine asymptotics. In fact, the numerical studies can do more and should do more. A natural question is whether we can find more such beautiful formulas in the tt^* equation via numerical study. The second part of this paper is devoted to the numerical study of the fine asymptotics of the solutions in an enlarged class defined from the Stoke data side. All the fine asymptotics of the solutions in the enlarged class are found by the numerical study. The success of the numerical study is largely due to the truncation structures of the tt^* equation.

1 Introduction

The tt^* equations were introduced by Cecotti and Vafa when they studied the fusion of topological $N = 2$ supersymmetric quantum field theory with its conjugate, the anti-topological one [1]. They also appeared in the extraction of exact results for supersymmetric σ models [2] and in the classification of the $N = 2$ supersymmetric theories [3]. Dubrovin gave the zero-curvature representation of the tt^* equations and studied their geometrical aspects [4]. An important special class of the tt^* equations are the tt^* -Toda equations, which are the reduction of the two-dimensional $(n + 1)$ -periodic Toda lattice with opposite sign

$$\begin{cases} 2(w_i)_{z\bar{z}} = -e^{2(w_{i+1}-w_i)} + e^{2(w_i-w_{i-1})} \\ w_{i+n+1} = w_i \end{cases}, \quad (1)$$

where \bar{z} denotes the complex conjugate of $z \in \mathbb{C}$ and $w_i = w_i(z, \bar{z}) \in \mathbb{R}$, constrained by both the l -anti-symmetry constraint

$$\begin{cases} w_0 + w_{l-1} = 0, & w_1 + w_{l-2} = 0, & \dots \\ w_l + w_n = 0, & w_{l+1} + w_{n-1} = 0, & \dots \end{cases}, \quad (2)$$

where the fixed $l \in \{0, 1, \dots, n\}$, and the radial constraint

$$w_i(z, \bar{z}) = w_i(|z|), \quad i \in \{0, 1, \dots, n\}. \quad (3)$$

The $l = 0$ case of tt^* -Toda equations is called the A_n type. They were first derived by Cecotti and Vafa when they deformed the superpotentials with the A_n -minimal model of the Landau-Ginzburg approach [1]. The existence of global solutions for any n for these A_n type tt^* -Toda equations can be established by the Higgs bundle method [10, 11]. Recently, the existence and uniqueness of these solutions were proved using the Riemann-Hilbert method [8].

Almost all concrete example studies of the tt^* equations were reduced to the third Painlevé equation before the work of Guest and Lin [9], where they initiated the direct study of a generalized tt^* equation with two unknowns

$$\begin{cases} u_{z\bar{z}} = e^{au} - e^{v-u} \\ v_{z\bar{z}} = e^{v-u} - e^{-bv} \end{cases}, \quad (4)$$

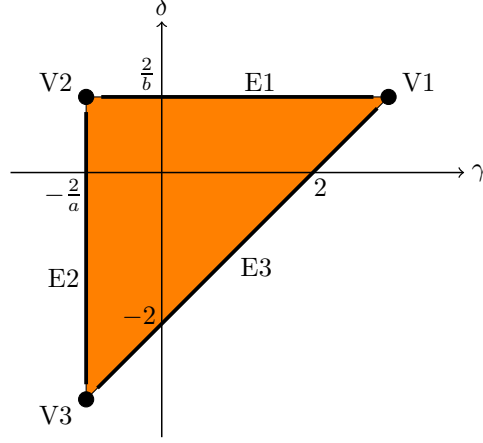


Figure 1: The triangular region for (γ, δ) .

where $a, b > 0$, subject to the boundary condition

$$\begin{cases} u(z) \xrightarrow{|z| \rightarrow \infty} 0, & v(z) \xrightarrow{|z| \rightarrow \infty} 0 \\ u(z) \xrightarrow{z \rightarrow 0} (\gamma + o(1)) \log |z|, & v(z) \xrightarrow{z \rightarrow 0} (\delta + o(1)) \ln |z| \end{cases}. \quad (5)$$

The tt^* -Toda equations with two dependent variables are the cases $a, b \in \{1, 2\}$, exhausted in [9].

In [5], Guest, Its and Lin proved the following property for Equation (4) with boundary condition (5).

Theorem 1.1. [5] *For $a, b > 0$ and any (γ, δ) in the triangular region*

$$\gamma \geq -\frac{2}{a}, \quad \delta \leq \frac{2}{b}, \quad \gamma - \delta \leq 2,$$

the system (4) has a unique smooth solution that satisfies the boundary condition (5). Furthermore, the unique solution is real and radially-invariant.

Theorem 1.1 establishes a map from the point (γ, δ) in the triangular region in Figure 1 to the smooth solution of Equation (4). Thus, it characterizes a two-parameter family of smooth real solutions of the tt^* equation in \mathbb{C}^* . Note that a result similar to Theorem 1.1 had been obtained by Guest and Lin in [9], where they required $\gamma, \delta > 0$. But the difference is crucial since Theorem 1.1 characterizes *all* smooth radial solution of Equation (4) [6]. By the Riemann-Hilbert approach, Guest et al. obtained all connection formulae for the tt^* cases, i.e., $a, b \in \{1, 2\}$ [6]. The complete picture of the monodromy data, holomorphic data, and asymptotic data were finally obtained in [7].

The case $a = b = 2$ of (4), which is the case 4a in their classification of the tt^* -Toda equations, was studied more thoroughly. In [7], the fine asymptotics (see below for the exact definition) are all given for the class of solutions defined in Theorem 1.1. In this case, $w_0 = \frac{1}{2}u$ and $w_1 = \frac{1}{2}v$ were used as the proper independent variables. Then (4) becomes

$$\begin{cases} 2(w_0)_{z\bar{z}} = e^{4w_0} - e^{2w_1-2w_0} \\ 2(w_1)_{z\bar{z}} = e^{2w_1-2w_0} - e^{-4w_1} \end{cases}. \quad (6)$$

According to the radical constraint (3), system (6) is written into an ordinary differential equations (ODEs) with variable $r = |z|$

$$\begin{cases} \frac{1}{2}w_0'' + \frac{1}{2r}w_0' = e^{4w_0} - e^{2w_1-2w_0} \\ \frac{1}{2}w_1'' + \frac{1}{2r}w_1' = e^{2w_1-2w_0} - e^{-4w_1} \end{cases}, \quad (7)$$

where the prime denotes $\frac{d}{dr}$. Near $r = 0$, by (5), w_0 and w_1 have properties

$$\begin{cases} 2w_0(r) \xrightarrow{r \rightarrow 0} (\gamma_0 + o(1)) \ln r \\ 2w_1(r) \xrightarrow{r \rightarrow 0} (\gamma_1 + o(1)) \ln r \end{cases}. \quad (8)$$

Near $r = \infty$, the asymptotics of w_0 and w_1 are expressed by the Stokes data $s_1^{\mathbb{R}}$ and $s_2^{\mathbb{R}}$ [6]:

$$\begin{cases} w_0(r) + w_1(r) \xrightarrow{r \rightarrow \infty} -s_1^{\mathbb{R}} 2^{-\frac{3}{4}} (\pi r)^{-\frac{1}{2}} e^{-2\sqrt{2}r} \\ w_0(r) - w_1(r) \xrightarrow{r \rightarrow \infty} s_2^{\mathbb{R}} 2^{-\frac{3}{2}} (\pi r)^{-\frac{1}{2}} e^{-4r} \end{cases}. \quad (9)$$

The map from (γ_0, γ_1) to $(s_1^{\mathbb{R}}, s_2^{\mathbb{R}})$ is the connection formula [6]

$$\begin{cases} s_1^{\mathbb{R}} = -2 \cos\left(\frac{\pi}{4}(\gamma_0 + 1)\right) - 2 \cos\left(\frac{\pi}{4}(\gamma_1 + 3)\right) \\ s_2^{\mathbb{R}} = -2 - 4 \cos\left(\frac{\pi}{4}(\gamma_0 + 1)\right) \cos\left(\frac{\pi}{4}(\gamma_1 + 3)\right) \end{cases}. \quad (10)$$

The $r = \infty$ asymptotics (9) is able to uniquely fix the solution of (7). This is an initial value problem from $r = \infty$. However, the rough asymptotics (8) itself is not enough to fix the solution. To fix the solution, it must be accompanied by the rough asymptotics at $r = \infty$: $w_0(r) \xrightarrow{r \rightarrow \infty} 0$, $w_1(r) \xrightarrow{r \rightarrow \infty} 0$. But this becomes a boundary value problem. To get an initial value problem from $r = 0$, one should start with a more detailed asymptotics near $r = 0$. In fact, it would be very appropriate to start with the fine asymptotics at $r = 0$.

Definition 1.2. *An asymptotics is said to be a fine asymptotics of a system of differential equations if it satisfies the system's truncation equation with respect to the asymptotics.*

As an example, let us find out the fine asymptotics of (7) at $r = \infty$ that coincides with asymptotics (9). The truncation equation for the solutions of (7) with respect to the asymptotics $w_0(r) \rightarrow 0$ and $w_1(r) \rightarrow 0$ is

$$\begin{cases} \frac{1}{2}w_0'' + \frac{1}{2r}w_0' = 6w_0 - 2w_1 \\ \frac{1}{2}w_1'' + \frac{1}{2r}w_1' = 6w_1 - 2w_0 \end{cases}. \quad (11)$$

The exact solution of (11) that coincides with asymptotics (9) is

$$\begin{cases} w_0(r) + w_1(r) = -\frac{\sqrt{2}}{\pi} s_1^{\mathbb{R}} K_0(2\sqrt{2}r) \\ w_0(r) - w_1(r) = \frac{1}{\pi} s_2^{\mathbb{R}} K_0(4r) \end{cases}, \quad (12)$$

where K_0 denotes the Bessel K_0 function. So (12) is the fine asymptotics for the solutions with asymptotics $w_0(r) \rightarrow 0$ and $w_1(r) \rightarrow 0$ at $r = \infty$, whereas asymptotics (9) should not be taken as a fine asymptotics since it is not an exact solution of (11).

In [7], all fine asymptotics of (7) at $r = 0$ for the solutions described by Theorem 1.1 have been obtained. These fine asymptotics contain seven cases. For convenience, we list them in Section 2. Therefore, the fine asymptotics at $r = \infty$ and $r = 0$ are all known for the solutions described by Theorem 1.1, i.e., the situations at $r = \infty$ and $r = 0$ become symmetric.

However, these fine asymptotics at $r = 0$ are complicated, especially that of the vertex case. An intuitive explanation is still lacking. No similar result can be compared except for the general case. This is our motivation to start the numerical study. The first part of this paper verifies these fine asymptotics numerically up to 100 digits for all the seven cases at $r = 0$.

Fine asymptotics are subject to the class of the solutions. If the solution class is enlarged, new fine asymptotics will appear. We will enlarge the solution class from the Stoke data side in the following way. The connection formula (10) maps the (γ_0, γ_1) region to the $(s_1^{\mathbb{R}}, s_2^{\mathbb{R}})$ region. Coming down to Equation (7), the region map can be represented by Figure 2. Any solution represented by a point $(s_1^{\mathbb{R}}, s_2^{\mathbb{R}})$ in the curved triangle (including the edges and the vertexes) in Figure 2 must have asymptotic (13) near $r = 0$, where (γ_0, γ_1) is determined by $(s_1^{\mathbb{R}}, s_2^{\mathbb{R}})$ by the connection formula (10). So the class of solutions described by Theorem 1.1 are parameterized by the points in the curved triangle (including the edges and the vertexes). We enlarge the class of solutions to the ones parameterized by the points on the whole real $(s_1^{\mathbb{R}}, s_2^{\mathbb{R}})$ plane. Based on our numerical results, we will generalize the range and the explanation of the connection formula and obtain all the fine asymptotics of the enlarged class of solutions at $r = 0$. Of course, the solution class can also be generalized from the side of $r = \infty$. However, the problem is much harder to solve.

The paper is organized as follows. In Section 2, we list all the seven fine asymptotics of (7) at $r = 0$ obtained in [7]. In Section 3, we numerically verify these seven fine asymptotics. In Section 4, we study the cases where $(s_1^{\mathbb{R}}, s_2^{\mathbb{R}})$ is outside the curved triangle and obtain our main result. In Section 5, we present a numerical study from the $r = 0$ side. In Section 6, we give the conclusion and discussions. This paper can be seen as a complement [5, 6, 7].

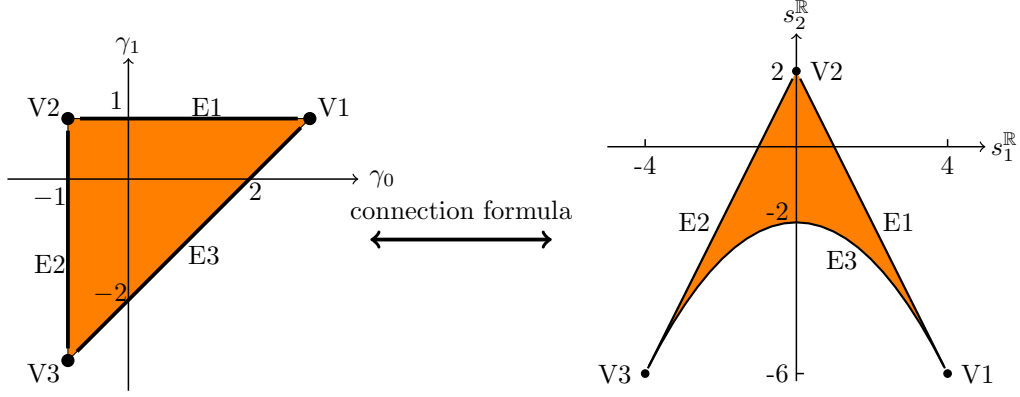


Figure 2: The region map of the connection formula (10).

2 Fine asymptotics of (7) at $r = 0$ of the class of solutions defined by Theorem 1.1

The fine asymptotics of (7) at $r = 0$ of the class of solutions defined by Theorem 1.1 have all been obtained in [7]. For convenience, we list them all here. We will use the following notations.

- Γ : $\Gamma(z)$ is the usual Gamma function defined by $\Gamma(z) = \int_0^{+\infty} t^{z-1} e^{-t} dt$ for $\Re(z) > 0$.
- ψ : $\psi(z) = \frac{d}{dz} \ln(\Gamma(z)) = \frac{\Gamma'(z)}{\Gamma(z)}$.
- s : $s = -\ln(r)$ is used as an easy independent variable near $r = 0$.
- γ_{EU} : γ_{EU} is the Euler's constant γ , whose numerical values is approximately 0.5772156649.
- ζ : $\zeta(z)$ is the Riemann zeta function.

The seven fine asymptotics of (7) at $r = 0$ obtained in [7] are the following.

- General case:

$$\begin{cases} 2w_0(r) \xrightarrow{r \rightarrow 0} \gamma_0 \ln r + \rho_0 \\ 2w_1(r) \xrightarrow{r \rightarrow 0} \gamma_1 \ln r + \rho_1 \end{cases}, \quad (13)$$

where

$$\begin{cases} \rho_0 = -\ln \left(2^{2\gamma_0} \frac{\Gamma(\frac{1+\gamma_0}{4}) \Gamma(\frac{4+\gamma_0+\gamma_1}{8}) \Gamma(\frac{6+\gamma_0-\gamma_1}{8})}{\Gamma(\frac{3-\gamma_0}{4}) \Gamma(\frac{4-\gamma_0-\gamma_1}{8}) \Gamma(\frac{2-\gamma_0+\gamma_1}{8})} \right) \\ \rho_1 = -\ln \left(2^{2\gamma_1} \frac{\Gamma(\frac{3+\gamma_1}{4}) \Gamma(\frac{4+\gamma_0+\gamma_1}{8}) \Gamma(\frac{2-\gamma_0+\gamma_1}{8})}{\Gamma(\frac{1-\gamma_1}{4}) \Gamma(\frac{4-\gamma_0-\gamma_1}{8}) \Gamma(\frac{6+\gamma_0-\gamma_1}{8})} \right) \end{cases}. \quad (14)$$

- E1 case:

$$\begin{cases} 2w_0(r) \xrightarrow{r \rightarrow 0} \gamma_0 \ln r + a_{E1} \\ 2w_1(r) \xrightarrow{r \rightarrow 0} \ln r + \ln(-2s + b_{E1}) \end{cases}, \quad (15)$$

where

$$\begin{aligned} a_{E1} &= -\ln \left(2^{2\gamma_0} \frac{\Gamma(\frac{\gamma_0+1}{4}) \left(\Gamma(\frac{\gamma_0+5}{8}) \right)^2}{\Gamma(\frac{3-\gamma_0}{4}) \left(\Gamma(\frac{3-\gamma_0}{8}) \right)^2} \right), \\ b_{E1} &= \frac{1}{2} \psi\left(\frac{3-\gamma_0}{8}\right) + \frac{1}{2} \psi\left(\frac{5+\gamma_0}{8}\right) - \gamma_{eu} + 4 \ln 2. \end{aligned}$$

- E2 case:

$$\begin{cases} 2w_0(r) \xrightarrow{r \rightarrow 0} -\ln(r) - \ln(-2s + a_{E2}) \\ 2w_1(r) \xrightarrow{r \rightarrow 0} \gamma_1 \ln(r) + b_{E2} \end{cases}, \quad (16)$$

where

$$a_{E2} = \frac{1}{2}\psi\left(\frac{3+\gamma_1}{8}\right) + \frac{1}{2}\psi\left(\frac{5-\gamma_1}{8}\right) - \gamma_{eu} + 4\ln 2,$$

$$b_{E2} = -\ln\left(2^{2\gamma_1}\frac{\Gamma\left(\frac{\gamma_1+3}{4}\right)\left(\Gamma\left(\frac{\gamma_1+3}{8}\right)\right)^2}{\Gamma\left(\frac{1-\gamma_1}{4}\right)\left(\Gamma\left(\frac{5-\gamma_1}{8}\right)\right)^2}\right).$$

- E3 case:

$$\begin{cases} 2w_0(r) + 2w_1(r) \xrightarrow{r \rightarrow 0} 2(\gamma_0 - 1)\ln(r) + a_{E3} \\ 2w_1(r) - 2w_0(r) \xrightarrow{r \rightarrow 0} -2\ln(r) - \ln(4(s + b_{E3})^2) \end{cases}, \quad (17)$$

where

$$a_{E3} = 4(1 - \gamma_0)\ln 2 - 4\ln\left(\Gamma\left(\frac{1+\gamma_0}{4}\right)\right) + 4\ln\left(\Gamma\left(\frac{3-\gamma_0}{4}\right)\right),$$

$$b_{E3} = -\frac{1}{4}\psi\left(\frac{3-\gamma_0}{4}\right) - \frac{1}{4}\psi\left(\frac{\gamma_0-3}{4}\right) + \frac{1}{3-\gamma_0} + \frac{\gamma_{EU}}{2} - 2\ln(2). \quad (18)$$

- V1 case:

$$\begin{cases} 2w_0(r) \xrightarrow{r \rightarrow 0} 3\ln(r) + \ln(P_3) \\ 2w_0(r) + 2w_1(r) \xrightarrow{r \rightarrow 0} 4\ln(r) + \ln(P_4) \end{cases}, \quad (19)$$

where

$$P_3 = -\frac{4}{3}(s - \ln 4)^3 - 4\gamma_{eu}(s - \ln 4)^2 - 4\gamma_{eu}^2(s - \ln 4) - \frac{1}{24}\zeta(3) - \frac{4}{3}\gamma_{eu}^3, \quad (20)$$

$$P_4 = \frac{4}{3}(s - \ln 4)^4 + \frac{16}{3}\gamma_{eu}(s - \ln 4)^3 + 8\gamma_{eu}^2(s - \ln 4)^2 + \left(\frac{16\gamma_{eu}^3}{3} - \frac{\zeta(3)}{12}\right)(s - \ln 4) - \frac{\gamma_{eu}\zeta(3)}{12} + \frac{4\gamma_{eu}^4}{3}. \quad (21)$$

- V2 case:

$$2w_0(r) = -2w_1(r) \xrightarrow{r \rightarrow 0} -\ln(r) - \ln(-2s - 2\gamma_{eu} + 2\ln 2). \quad (22)$$

- V3 case:

$$\begin{cases} 2w_1(r) \xrightarrow{r \rightarrow 0} -3\ln(r) - \ln(P_3) \\ 2w_0(r) + 2w_1(r) \xrightarrow{r \rightarrow 0} -4\ln(r) - \ln(P_4) \end{cases}, \quad (23)$$

where P_3 and P_4 are defined by (20) and (21).

3 Verifying numerically the fine asymptotics of (7) at $r = 0$ of the class of solutions defined by Theorem 1.1

It is well known that Equation (7) has symmetry

$$\begin{cases} w_0 \rightarrow -w_1 \\ w_1 \rightarrow -w_0 \end{cases},$$

i.e., if $(w_0(r), w_1(r)) = (f(r), g(r))$ is a solution of the tt* equation, then $(w_0(r), w_1(r)) = (-g(r), -f(r))$ is also a solution of the tt*. Therefore, if the solution $(w_0(r), w_1(r)) = (f(r), g(r))$ has data $(\gamma_0, \gamma_1) = (\mu_0, \mu_1)$ and $(s_1^{\mathbb{R}}, s_2^{\mathbb{R}}) = (\nu_1, \nu_2)$, then the solution $(w_0(r), w_1(r)) = (-g(r), -f(r))$ will have data $(\gamma_0, \gamma_1) = (-\mu_0, -\mu_1)$ and $(s_1^{\mathbb{R}}, s_2^{\mathbb{R}}) = (-\nu_1, \nu_2)$ by (8) and (9). From this symmetry, the fine asymptotics of the E2 case and the V3 case can be obtained from those of the E1 case and the V1 case respectively. Furthermore, as has been mentioned in [7], the V2 case is just the sinh-Gordon, for which the asymptotic is already well known. So, we will only verify four cases: the general, E1, E3 and V1. Instead of verifying these asymptotics directly, which is difficult to reach a satisfactory accuracy, we will find out the associated truncation of (7) for the asymptotics and use the truncation to verify the asymptotics. Numerical results show that the verifications achieve high accuracy.

3.1 Preliminary for the numerical experiments: an approximation proper for calculations near $r = \infty$

Consider the solutions of (7) with asymptotics $w_0(r) \xrightarrow{r \rightarrow \infty} 0$ and $w_1(r) \xrightarrow{r \rightarrow \infty} 0$. Near $r = \infty$ the primary asymptotics of the solutions is given by the fine asymptotics (12).

Let

$$\begin{cases} w_p = w_0 + w_1 \\ w_m = w_0 - w_1 \end{cases} . \quad (24)$$

Then, the equations for w_p and w_m are

$$\begin{cases} \left(\frac{1}{2} \frac{d^2}{dr^2} + \frac{1}{2r} \frac{d}{dr} \right) w_p = e^{2w_p+2w_m} - e^{2w_p-2w_m} = 2e^{2w_m} \sinh(2w_p) \\ \left(\frac{1}{2} \frac{d^2}{dr^2} + \frac{1}{2r} \frac{d}{dr} \right) w_m = e^{2w_p+2w_m} + e^{2w_m-2w_p} - 2e^{-2w_m} = 4e^{2w_m} \sinh^2(w_p) + 4 \sinh(2w_m) \end{cases} . \quad (25)$$

Note that (25) is written in a form that better preserves the significant digits in the numerical integration near $r = \infty$. The errors in the approximation of (w_p, w_m) by the fine asymptotics (12) are caused by the nonlinear terms in the expansion of (25). In general, the most significant correction to w_p is proportional to $w_p^L w_m^L$, i.e., $w_p = c_p K_0(2\sqrt{2}r) + O(r^{-1}e^{-(2\sqrt{2}+4)r})$. Meanwhile, the most significant correction to w_m is proportional to the square of w_p^L , i.e., $w_m = c_m K_0(4r) + O(r^{-1}e^{-4\sqrt{2}r})$.

These results are sufficient for the rough numerical investigations for smooth solutions of the tt* equation. They are called rough simply because they can be refined. For high precision numerical integration of (25) from the $r = \infty$ side, the relative error will not enlarge too much when r is still large. For $w_m(r)$, the relative error is about $O(r^{-\frac{1}{2}}e^{-4(\sqrt{2}-1)r})$. If we give the initial values by the fine asymptotics (12) with $r = 45$, the relative error of the initial values are of order 10^{-33} , which is not so satisfactory. If we want to reach a relative error of order 10^{-100} by this way, $r = 138$ is needed to give the initial values. We will see, after considering the most significant contribution of the nonlinear terms, the starting r can be greatly reduced.

Suppose

$$\begin{cases} w_p(r) = w_p^{(0)}(r) + w_p^{(1)}(r) + w_p^{(2)}(r) + \dots \\ w_m(r) = w_m^{(0)}(r) + w_m^{(1)}(r) + w_m^{(2)}(r) + \dots \end{cases} ,$$

where

$$\begin{cases} w_p^{(0)}(r) = -\frac{\sqrt{2}}{\pi} s_1^{\mathbb{R}} K_0(2\sqrt{2}r) \\ w_m^{(0)}(r) = \frac{1}{\pi} s_2^{\mathbb{R}} K_0(4r) \end{cases} . \quad (26)$$

Then $w_p^{(1)}$ and $w_m^{(1)}$ satisfy

$$\begin{cases} \left(\frac{1}{2} \frac{d^2}{dr^2} + \frac{1}{2r} \frac{d}{dr} \right) w_p^{(1)} - 4w_p^{(1)} = 8w_p^{(0)} w_m^{(0)} \\ \left(\frac{1}{2} \frac{d^2}{dr^2} + \frac{1}{2r} \frac{d}{dr} \right) w_m^{(1)} - 8w_m^{(1)} = 4(w_p^{(0)})^2 \end{cases}$$

with $w_p^{(1)}(\infty) = 0$ and $w_m^{(1)}(\infty) = 0$.

The solution of $w_p^{(1)}$ and $w_m^{(1)}$ is:

$$\begin{cases} w_p^{(1)} = 2I_0(2\sqrt{2}r) \int_{\infty}^r K_0(2\sqrt{2}r) \left(8w_p^{(0)}(r) w_m^{(0)}(r) \right) r dr - 2K_0(2\sqrt{2}r) \int_{\infty}^r I_0(2\sqrt{r}) \left(8w_p^{(0)}(r) w_m^{(0)}(r) \right) r dr \\ w_m^{(1)} = 2I_0(4r) \int_{\infty}^r K_0(4r) \left(4(w_p^{(0)}(r))^2 \right) r dr - 2K_0(4r) \int_{\infty}^r I_0(4r) \left(4(w_p^{(0)}(r))^2 \right) r dr \end{cases} .$$

Then

$$\begin{cases} w_p(r) = w_p^{(0)}(r) + w_p^{(1)}(r) + O\left(r^{-\frac{3}{2}}e^{-6\sqrt{2}r}\right) \\ w_m(r) = w_m^{(0)}(r) + w_m^{(1)}(r) + O\left(r^{-\frac{3}{2}}e^{-(4+4\sqrt{2})r}\right) \end{cases} . \quad (27)$$

The relative errors are both of order $r^{-1}e^{-4\sqrt{2}r}$. To acquire a relative error of order 10^{-100} , it is enough to start the numerical integration from $r = 45$. Higher-order nonlinear terms should not be considered, otherwise we will run into high-dimensional integrations that are time-consuming to compute to high accuracy, for example, an accuracy of 10^{-100} .

The truncation of (27) will be used to give initial values for the numerical integration of (25) near $r = \infty$ for all of the following cases.

3.2 The general case: in the triangular

This subsection is devoted to the verification of (13).

To be specific, we fix $(\gamma_0, \gamma_1) = (1, \frac{1}{3})$. Then, $(s_1^{\mathbb{R}}, s_2^{\mathbb{R}}) = (\sqrt{3}, -2)$ by (10). (27) means that we can start our numerical integration from $r = 45$ for moderate $(s_1^{\mathbb{R}}, s_2^{\mathbb{R}})$ to get a relative error of order less than 10^{-100} . Recall that in Section 2 we have mentioned

$$s = \ln r \quad (28)$$

is a proper independent variable near $r = 0$. Therefore, the numerical integration is naturally divided into two parts: on $r \in [r_m, 45]$ and on $s \in [s_f, s_m = \ln r_m]$. For convenience, we always choose $r_m = 1$. s_f varies with $(s_1^{\mathbb{R}}, s_2^{\mathbb{R}})$ and will be determined after we solve the associated truncation of (7) for the fine asymptotics.

3.2.1 Numerical integration from $r = 45$ to $r = 1$

By the truncation of (27), the initial values for the numerical integration of (25) are calculated up to more than 100 digits

$$\begin{cases} w_p(45) = -4.5763465910740842210810671823515633075572030760030... \times 10^{-57} \\ w'_p(45) = 1.2994612025622450236510718743064448909150132699101... \times 10^{-56} \\ w_m(45) = -3.9902150828859022626192436154419670328254784177405... \times 10^{-80} \\ w'_m(45) = 1.6005134816454403480052616718328017176197600655449... \times 10^{-79} \end{cases} \quad (29)$$

To save space, we list only the first 50 digits in (29). It is not surprising that $w_m(45)$ in (29) coincides with $w_m^0(45) = -\frac{\sqrt{6}}{\pi}K_0(90\sqrt{2})$ for the first 33 digits and that $w_p(45)$ in (29) coincides with $w_p^0(45) = -\frac{2}{\pi}K_0(180)$ for all the listed 50 digits. Formula (27) gives only the order of the error, not the actual value. We obtain the errors of (29) by comparing the initial values (29) with a more accurate numerical solution starting from $r = 55$. Table 1 shows both the absolute error and the relative error of the initial values at $r = 45$.

Table 1: Errors of the initial values for the general case with $(\gamma_0, \gamma_1) = (1, \frac{1}{3})$.

$r = 45$	w_p	w'_p	w_m	w'_m
— Absolute Error —	1.98×10^{-170}	1.68×10^{-169}	2.43×10^{-193}	2.36×10^{-192}
— Relative Error —	4.32×10^{-114}	1.30×10^{-113}	6.09×10^{-114}	1.47×10^{-113}

In this paper, we use the Gauss-Legendre method, which is an implicit Runge-Kutta method suitable for high-precision numerical integration, to numerically integrate ODEs. Integrating (25) numerically from $r = 45$ to $r = 1$ by a 100-stage Gauss-Legendre method with step size $\frac{1}{100}$, we obtain the numerical values of w_p , w'_p , w_m and w'_m at $r = 1$:

$$\begin{cases} w_p(1) = -3.2972969594742103001480456261339460432792854660454... \times 10^{-2} \\ w'_p(1) = 1.0829838290019404254859616425541702465151021916881... \times 10^{-1} \\ w_m(1) = -6.6648017026562016812805168052539563362254856278250... \times 10^{-3} \\ w'_m(1) = 2.8961723214345113722967491163879906375020596216242... \times 10^{-2} \end{cases} \quad (30)$$

Note that (30) only lists the first 50 digits of the numerical solution. Numerical experiments show that the errors caused by the numerical integration are all negligible. This is easy to understand because the precision order of the numerical integration, which is twice the stage number, is large and the step size is small.

Comparing (30) with the more accurate solution starting from $r = 55$, we obtain the errors of (30) as Table 2.

Table 2: Errors of the numerical solution at $r = 1$ for the general case with $(\gamma_0, \gamma_1) = (1, \frac{1}{3})$.

$r = 1$	w_p	w'_p	w_m	w'_m
— Absolute Error —	2.85×10^{-115}	9.31×10^{-115}	6.64×10^{-116}	2.82×10^{-115}
— Relative Error —	8.63×10^{-114}	8.60×10^{-114}	9.97×10^{-114}	9.75×10^{-114}

3.2.2 Near $r = 0$

Inspired by the form of (13), we use independent variable s and dependent variables

$$\begin{cases} \tilde{w}_0 = 2w_0 - \gamma_0 s \\ \tilde{w}_1 = 2w_1 - \gamma_1 s \end{cases} \quad (31)$$

Please recall that $s = \ln(r)$ is defined by (28). From the numeric point of view, the advantage of using s rather than r is that it can avoid the frequent adjustment of the step size when we solve (7) numerically near $r = 0$.

The equations for \tilde{w}_0 and \tilde{w}_1 are

$$\begin{cases} \frac{1}{4} \frac{d^2 \tilde{w}_0}{ds^2} = e^{2\tilde{w}_0 + 2(\gamma_0 + 1)s} - e^{\tilde{w}_1 - \tilde{w}_0 + (\gamma_1 - \gamma_0 + 2)s} \\ \frac{1}{4} \frac{d^2 \tilde{w}_1}{ds^2} = e^{\tilde{w}_1 - \tilde{w}_0 + (\gamma_1 - \gamma_0 + 2)s} - e^{-2\tilde{w}_1 + 2(1 - \gamma_1)s} \end{cases} \quad (32)$$

We expect $\tilde{w}_0 \xrightarrow{s \rightarrow -\infty} \rho_0$ and $\tilde{w}_1 \xrightarrow{s \rightarrow -\infty} \rho_1$. In the triangular, $\gamma_0 > -1$, $\gamma_1 < 1$, $\gamma_1 > \gamma_0 - 2$. So, all terms in the right of (32) can be ignored at first. Thus,

$$\begin{cases} \frac{1}{4} \frac{d^2 \tilde{w}_0^{(0)}}{ds^2} = 0 \\ \frac{1}{4} \frac{d^2 \tilde{w}_1^{(0)}}{ds^2} = 0 \end{cases} \quad (33)$$

is the associated truncation of (32) for the fine asymptotics of the general case.

The initial values of \tilde{w}_0 , $\frac{d\tilde{w}_0}{ds}$, \tilde{w}_1 and $\frac{d\tilde{w}_1}{ds}$ at $s = 0$ can be derived from w_p , w'_p , w_m and w'_m at $r = 1$:

$$\begin{cases} \tilde{w}_0|_{s=0} = w_p|_{r=1} + w_m|_{r=1} \\ \frac{d\tilde{w}_0}{ds}|_{s=0} = w'_p|_{r=1} + w'_m|_{r=1} - \gamma_0 \\ \tilde{w}_1|_{s=0} = w_p|_{r=1} - w_m|_{r=1} \\ \frac{d\tilde{w}_1}{ds}|_{s=0} = w'_p|_{r=1} - w'_m|_{r=1} - \gamma_1 \end{cases} \quad (34)$$

In the truncation of (32) to (33), the ignored terms are of order $O(e^{2(\gamma_0 + 1)s})$, order $O(e^{(\gamma_1 - \gamma_0 + 2)s})$ and order $O(e^{2(1 - \gamma_1)s})$. Now, we have fixed $(\gamma_0, \gamma_1) = (1, \frac{1}{3})$. Thus, $(\tilde{w}_0, \tilde{w}_1)$ will approach $(\rho_0, \rho_1)|_{\gamma_0=1, \gamma_1=\frac{1}{3}}$ with a distance of order $O(e^{\frac{4}{3}s})$, where

$$\begin{cases} \rho_0|_{\gamma_0=1, \gamma_1=\frac{1}{3}} = 0.89156581440748831917188012305422345475702308262231... \\ \rho_1|_{\gamma_0=1, \gamma_1=\frac{1}{3}} = 0.22017225140694662756648980530049931068839656816740... \end{cases}$$

by (14). So, when $e^{\frac{4}{3}s} \approx 10^{-100}$, i.e., $s \approx -172.7$, $(\tilde{w}_0, \tilde{w}_1)$ will be indistinguishable from $(\rho_0, \rho_1)|_{\gamma_0=1, \gamma_1=\frac{1}{3}}$ within our precision tolerance. Therefore, it is enough to integrate (32) numerically from $s = 0$ to $s_f = -175$.

Table 3: Errors of the numerical solution at $s = -175$ for the general case with $(\gamma_0, \gamma_1) = (1, \frac{1}{3})$.

$s = -175$	\tilde{w}_0	$\frac{d\tilde{w}_0}{ds}$	\tilde{w}_1	$\frac{d\tilde{w}_1}{ds}$
— Absolute Error —	1.33×10^{-111}	7.66×10^{-114}	6.54×10^{-112}	3.76×10^{-114}
— Relative Error —	1.50×10^{-111}	1.08×10^{-12}	2.97×10^{-111}	2.04×10^{-12}

Table 3 shows that the numerical solution is as accurate as we expected. The relative error of $\frac{d\tilde{w}_0}{ds}$ or $\frac{d\tilde{w}_1}{ds}$ in Table 3 seems to be large. But this is really nothing since it is only another demonstration of the fact that $\frac{d\tilde{w}_0}{ds}$ and $\frac{d\tilde{w}_1}{ds}$ are small.

Table 4 shows how good the asymptotic solution (13) is.

Table 4: Approximate derivation from the asymptotic solution for the general case with $(\gamma_0, \gamma_1) = (1, \frac{1}{3})$.

s	-25	-50	-75	-100	-125	-150	-175
$\ln(\rho_0 - \tilde{w}_0)$	-33.1938	-66.5271	-99.8605	-133.194	-166.527	-199.860	-233.194
$\ln(\rho_1 - \tilde{w}_1)$	-34.5412	-67.8745	-101.208	-134.541	-167.875	-201.208	-234.541

Table 4 not only numerically verifies the asymptotics of the general case for $(\gamma_0, \gamma_1) = (1, \frac{1}{3})$, but also confirms our estimate that $(\tilde{w}_0, \tilde{w}_1)$ is close to its asymptotics $(\rho_0, \rho_1)|_{\gamma_0=1, \gamma_1=\frac{1}{3}}$ with a distance of order $O(e^{\frac{4}{3}s})$.

3.3 Case E1

This subsection is devoted to the verification of the fine asymptotics of the E1 case. Note that the E1 case is parameterized by $-1 < \gamma_0 < 3$ and $\gamma_1 = 1$.

To fix the problem, we take $\gamma_0 = 1$ as an example to verify the E1 case. Substituting $(\gamma_0, \gamma_1) = (1, 1)$ to the connection formula (10), we immediately get $(s_1^{\mathbb{R}}, s_2^{\mathbb{R}}) = (2, -2)$. Similar to the general case of Subsection 3.2, the numerical integration is divided into two parts: for $r \in [1, 45]$ and for $s \in [s_f, 0]$.

3.3.1 Numerical integration from $r = 45$ to $r = 1$

By the truncation of (27), the initial values at $r = 45$ are obtained (only the first 50 digits are listed)

$$\begin{cases} w_p(45) = -5.2843098725232974899221393911204991207504443469367... \times 10^{-57} \\ w'_p(45) = 1.5004885502015739552694025310567337731833237644509... \times 10^{-56} \\ w_m(45) = -3.9902150828859022626192436154419666864562950795650... \times 10^{-80} \\ w'_m(45) = 1.6005134816454403480052616718328015209213735935410... \times 10^{-79} \end{cases} \quad (35)$$

Comparing with the more accurate solution starting from $r = 55$, the errors of the initial values (35) are obtained as shown by Table 5. Integrating (25) numerically from $r = 45$ to $r = 1$ by the Gauss-

Table 5: Errors of the initial values of case E1 with $\gamma_0 = 1$.

$r = 45$	w_p	w'_p	w_m	w'_m
— Absolute Error —	3.04×10^{-170}	2.59×10^{-169}	3.24×10^{-193}	3.14×10^{-192}
— Relative Error —	5.76×10^{-114}	1.73×10^{-113}	8.12×10^{-114}	1.96×10^{-113}

Legendre method with the same parameters as the ones in Subsection 3.2, the values of w_p , w'_p , w_m and w'_m at $r = 1$ are obtained

$$\begin{cases} w_p(1) = -3.8076020447615564848336037555396597913276640146800... \times 10^{-2} \\ w'_p(1) = 1.2507257120725277318359466237894266588814464453818... \times 10^{-1} \\ w_m(1) = -6.5181931373519405060356987540333399617643482502891... \times 10^{-3} \\ w'_m(1) = 2.8018632441288063804071518136255604932977444116709.... \times 10^{-2} \end{cases} \quad (36)$$

Comparing with the more accurate solution starting from $r = 55$, the errors of (36) are obtained as shown by Table 6.

Table 6: Errors of the numerical solution at $r = 1$ of case E1 with $\gamma_0 = 1$.

$r = 1$	w_p	w'_p	w_m	w'_m
— Absolute Error —	4.38×10^{-115}	1.43×10^{-114}	8.52×10^{-116}	3.55×10^{-115}
— Relative Error —	1.15×10^{-113}	1.15×10^{-113}	1.31×10^{-113}	1.27×10^{-113}

3.3.2 Near $r = 0$

Let

$$\begin{cases} \tilde{w}_0 = 2w_0 - \gamma_0 s \\ \tilde{w}_1 = 2w_1 - s \end{cases}, \quad (37)$$

where $s = \ln(r)$ as defined by (28). Then the differential equations for \tilde{w}_0 and \tilde{w}_1 are

$$\begin{cases} \frac{1}{4} \frac{d^2 \tilde{w}_0}{ds^2} = e^{2\tilde{w}_0 + 2(\gamma_0 + 1)s} - e^{\tilde{w}_1 - \tilde{w}_0 + (3 - \gamma_0)s} \\ \frac{1}{4} \frac{d^2 \tilde{w}_1}{ds^2} = e^{\tilde{w}_1 - \tilde{w}_0 + (3 - \gamma_0)s} - e^{-2\tilde{w}_1} \end{cases}. \quad (38)$$

Note that (38) can also be obtained from (32) by substituting $\gamma_1 = 1$ to it.

We expect \tilde{w}_0 is of order $O(1)$ and that \tilde{w}_1 is of order $O(\ln(-s))$. Also considering $-1 < \gamma_0 < 3$, we obtain the associated truncation of (38) near $s = -\infty$ for the fine asymptotic of the E1 case

$$\begin{cases} \frac{1}{4} \frac{d^2 \tilde{w}_0^{(0)}}{ds^2} = 0 \\ \frac{1}{4} \frac{d^2 \tilde{w}_1^{(0)}}{ds^2} = -e^{-2\tilde{w}_1^{(0)}} \end{cases}. \quad (39)$$

The general solution of (39) is

$$\begin{cases} \tilde{w}_0^{(0)} = k_{0E1} + k_{1E1}s \\ \tilde{w}_1^{(0)} = \ln\left(\pm \frac{2}{k_{2E1}} \sinh(k_{2E1}(s + k_{3E1}))\right) \end{cases} \quad (40)$$

By (15) and (37), we know the fine asymptotics of (7) in the E1 case corresponds to $k_{0E1} = a_{E1}$, $k_{1E1} = 0$, $k_{2E1} \rightarrow 0$ and $k_{3E1} = b_{E1}$.

In the truncation from (38) to (39), the ignored term for the differential equation of \tilde{w}_1 is $e^{\tilde{w}_1 - \tilde{w}_0 + (3-\gamma_0)s}$, which is of order $O(se^{(3-\gamma_0)s})$. Similarly, the ignored terms for the differential equation of \tilde{w}_0 are of order $O(se^{(3-\gamma_0)s})$ and order $O(e^{2(\gamma_0+1)s})$. In the current numerical experiment, $\gamma_0 = 1$. Therefore, the difference between the asymptotic solution and the exact solution is of order $O(se^{2s})$. So, we should do high-precision numerical integration from $s = 0$ to about $s = s_f = -120$ since $120 \times e^{2 \times (-120)} \approx 7.055 \times 10^{-103}$. Similar to the general case of Subsection 3.2, the values of \tilde{w}_0 , $\frac{d\tilde{w}_0}{ds}$, \tilde{w}_1 and $\frac{d\tilde{w}_1}{ds}$ at $s = 0$ are obtained by formula (34). Then, numerically integrating (38) by the Gauss-Legendre method, the high-precision numerical solution is obtained. Comparing it with the more accurate numerical solution starting from $r = 55$, the errors of the numerical solution are obtained. Table 7 shows that the numerical so-

Table 7: Errors of the numerical solution at $s = -120$ for the E1 case with $\gamma_0 = 1$.

$s = -120$	\tilde{w}_0	$\frac{d\tilde{w}_0}{ds}$	\tilde{w}_1	$\frac{d\tilde{w}_1}{ds}$
— Absolute Error —	1.06×10^{-111}	8.84×10^{-114}	3.56×10^{-110}	5.94×10^{-112}
— Relative Error —	1.35×10^{-111}	6.84×10^{-112}	6.50×10^{-111}	7.12×10^{-110}

lution is as accurate as we expected. The large relative error of $\frac{d\tilde{w}_0}{ds}$ is nothing but the fact that $\frac{d\tilde{w}_0}{ds}|_{s=-120} \approx -1.29 \times 10^{-102}$ is small.

Table 8 shows how good the asymptotic solution (15) is.

Table 8: Approximate derivation from the asymptotic solution for the E1 case with $\gamma_0 = 1$.

s	-20	-40	-60	-80	-100	-120
$\ln(a_{E1} - \tilde{w}_0)$	-37.0566	-76.3821	-115.983	-155.698	-195.477	-235.296
$\ln(\tilde{w}_1 - \ln(-2s + b_{E1}))$	-37.0553	-76.3818	-115.983	-155.698	-195.477	-235.296

Table 8 not only numerically verifies the asymptotics of the E1 case for $\gamma_0 = 1$, but also confirms our estimate that $(\tilde{w}_0, \tilde{w}_1)$ differs with its asymptotic solution by an order of $O(se^{2s})$.

3.4 Case E2

In this case, $\gamma_0 = -1$ and $-3 < \gamma_1 < 1$. As explained in the beginning of Section 3, the fine asymptotics of the E2 case can be obtained from the E1 case. So we omit the numerical verification for this case.

3.5 Case E3

This subsection will verify numerically the fine asymptotics of the E3 case. Note that in this case $\gamma_1 = \gamma_0 - 2$ and $-1 < \gamma_0 < 3$. Also note that

$$a_{E3} = \lim_{\gamma_1 \rightarrow \gamma_0 - 2} (\rho_0(\gamma_0, \gamma_1) + \rho_1(\gamma_0, \gamma_1)),$$

where ρ_0 and ρ_1 are defined by (14).

Let us take $\gamma_0 = \frac{1}{3}$ as an example to verify (17) numerically. Then $(s_1^{\mathbb{R}}, s_2^{\mathbb{R}}) = (-2, -3)$. Similar to the general case of Subsection 3.2, the numerical integration is divided into two parts: for $r \in [1, 45]$ and for $s \in [s_f, 0]$.

3.5.1 Numerical integration from $r = 45$ to $r = 1$

By the truncation of (27), the initial values at $r = 45$ are obtained (only the first 50 digits are listed)

$$\begin{cases} w_p(45) = 5.2843098725232974899221393911204991207504443469367... \times 10^{-57} \\ w'_p(45) = -1.5004885502015739552694025310567337731833237644509... \times 10^{-56} \\ w_m(45) = -5.9853226243288533939288654231629507224228092956986... \times 10^{-80} \\ w'_m(45) = 2.4007702224681605220078925077492026747788333343193... \times 10^{-79} \end{cases} \quad (41)$$

It is not surprising that $w_p(45)$ and $w'_p(45)$ of (41) coincide with that of (35) with many digits since $s_1^{\mathbb{R}} = -2$ in the example for this case and $s_1^{\mathbb{R}} = 2$ in the example for the E1 case.

Comparing with the more accurate solution starting from $r = 55$, the errors of the initial values (41) are obtained as shown by Table 9.

Table 9: Errors of the initial values of case E3 with $\gamma_0 = \frac{1}{3}$.

$r = 45$	w_p	w'_p	w_m	w'_m
— Absolute Error —	3.04×10^{-170}	2.59×10^{-169}	4.86×10^{-193}	4.71×10^{-192}
— Relative Error —	5.76×10^{-114}	1.73×10^{-113}	8.12×10^{-114}	1.96×10^{-113}

Numerically integrating (25) from $r = 45$ to $r = 1$ by the Gauss-Legendre method with the same parameters as the ones in Subsection 3.2, the values of w_p , w'_p , w_m and w'_m at $r = 1$ are obtained

$$\begin{cases} w_p(1) = 3.8027004168653915145363303284447255846983739527888... \times 10^{-2} \\ w'_p(1) = -1.2469806975938122928142121636698878096900701362539... \times 10^{-1} \\ w_m(1) = -1.0071686775204061495316019356342162460012952192431... \times 10^{-2} \\ w'_m(1) = 4.3926896299159549125370306923225572137558540540015.... \times 10^{-2} \end{cases} \quad (42)$$

Comparing with the more accurate solution starting from $r = 55$, the errors of (42) are obtained as shown by Table 10.

Table 10: Errors of the numerical solution at $r = 1$ of case E3 with $\gamma_0 = \frac{1}{3}$.

$r = 1$	w_p	w'_p	w_m	w'_m
— Absolute Error —	4.37×10^{-115}	1.42×10^{-114}	1.35×10^{-115}	5.76×10^{-115}
— Relative Error —	1.15×10^{-113}	1.14×10^{-113}	1.34×10^{-113}	1.31×10^{-113}

3.5.2 Near $r = 0$

Near $r = 0$, we still use the transformation (31). So the differential equations for \tilde{w}_0 and \tilde{w}_1 are also (32).

We expect \tilde{w}_0 and \tilde{w}_1 are of order $o(s)$. Also considering $-1 < \gamma_0 < 3$ and $\gamma_1 = \gamma_0 - 2$, we get the associated truncation of (32) near $s = -\infty$ for the E3 case:

$$\begin{cases} \frac{1}{4} \frac{d^2 \tilde{w}_0^{(0)}}{ds^2} = -e^{\tilde{w}_1 - \tilde{w}_0} \\ \frac{1}{4} \frac{d^2 \tilde{w}_1^{(0)}}{ds^2} = e^{\tilde{w}_1 - \tilde{w}_0} \end{cases} \quad (43)$$

The solution of (43) is

$$\begin{cases} \tilde{w}_0^{(0)} + \tilde{w}_1^{(0)} = k_{0E3} + k_{1E3}s \\ \tilde{w}_1^{(0)} - \tilde{w}_0^{(0)} = \ln \left(-\frac{k_{2E3}^2}{8 \pm 8 \cosh(k_{2E3}(s + k_{3E3}))} \right) \end{cases} \quad (44)$$

By (17) and (31), we know that the fine asymptotics of the E3 case is fixed by $k_{0E3} = a_{E1}$, $k_{1E3} = 0$, $k_{2E3} \rightarrow 0$ and $k_{3E3} = b_{E1}$.

In the truncation from (32) to (43), the ignored terms for the differential equation of $\tilde{w}_0 + \tilde{w}_1$ are $e^{2\tilde{w}_0 + 2(\gamma_0 + 1)s}$ and $e^{-2\tilde{w}_1 + 2(1 - \gamma_1)s}$, which are of order $O(s^2 e^{2(\gamma_0 + 1)s})$ and order $O(s^{-2} e^{2(\gamma_0 + 1)s})$. Similarly, the ignored terms for the differential equation of \tilde{w}_1 are also of order $O(s^{-2} e^{2(3 - \gamma_0)s})$ and order $O(s^{-2} e^{2(\gamma_0 + 1)s})$. In the current numerical experiment, $\gamma_0 = \frac{1}{3}$. Therefore, the difference between the asymptotic solution and the exact solution is of order $O(s^2 e^{\frac{8}{3}s})$. So, we should do high-precision numerical integration from $s = 0$ to about $s = s_f = -90$ since $90^2 \times e^{\frac{8}{3} \times (-90)} \approx 4.76 \times 10^{-101}$. Just as the general case, the values of \tilde{w}_0 , $\frac{d\tilde{w}_0}{ds}$, \tilde{w}_1 and $\frac{d\tilde{w}_1}{ds}$ at $s = 0$ are obtained by formula (34). Then, the high-precision numerical solution is obtained by numerically integrating (32) by the Gauss-Legendre method. Comparing it with the more accurate numerical solution starting from $r = 55$, the errors of the numerical solution are obtained. Table 11 shows that the numerical solution is as accurate as we expected.

Table 12 shows how good the asymptotic solution (17) is.

Table 11: Errors of the numerical solution at $s = -90$ for the E3 case with $\gamma_0 = \frac{1}{3}$.

$s = -90$	\tilde{w}_0	$\frac{d\tilde{w}_0}{ds}$	\tilde{w}_1	$\frac{d\tilde{w}_1}{ds}$
— Absolute Error —	1.30×10^{-110}	2.95×10^{-112}	1.41×10^{-110}	3.08×10^{-112}
— Relative Error —	2.74×10^{-111}	2.66×10^{-110}	2.51×10^{-111}	2.77×10^{-110}

 Table 12: Approximate derivation from the asymptotic solution for the E3 case with $\gamma_0 = \frac{1}{3}$.

s	-15	-30	-45	-60	-75	-90
$\ln(\tilde{w}_0 + \tilde{w}_1 - a_{E3})$	-34.5568	-73.2186	-112.424	-151.857	-191.415	-231.054
$\ln(\tilde{w}_0 - \tilde{w}_1 - \ln(4(s + b_{E3})^2))$	-34.5556	-73.2183	-112.424	-151.857	-191.415	-231.054

Table 12 not only numerically verifies the asymptotics of the E3 case for $\gamma_0 = \frac{1}{3}$, but also confirms our estimate that $\tilde{w}_0 + \tilde{w}_1$ and $\tilde{w}_1 - \tilde{w}_0$ deviate from their asymptotics by an order of $O(s^2 e^{\frac{8}{3}s})$. More detailed analysis shows that \tilde{w}_0 and \tilde{w}_1 deviate from their asymptotics by an order of $O(s^2 e^{\frac{8}{3}s})$ and an order of $O(e^{\frac{8}{3}s})$, respectively.

3.6 Case V1

This subsection is devoted to the verification of the fine asymptotics of the V1 case. Note that $\gamma_0 = 3$ and $\gamma_1 = 1$ in this case.

$(s_1^{\mathbb{R}}, s_2^{\mathbb{R}}) = (4, -6)$ by (10). Similar to the general case of Subsection 3.2, the numerical integration is done on two intervals: $r \in [1, 45]$ and $s \in [s_f, 0]$.

3.6.1 Numerical integration from $r = 45$ to $r = 1$

By the truncation of (27), the initial values at $r = 45$ are obtained (only the first 50 digits are listed)

$$\begin{cases} w_p(45) = -1.0568619745046594979844278782240998241500888693873... \times 10^{-56} \\ w'_p(45) = 3.0009771004031479105388050621134675463666475289019... \times 10^{-56} \\ w_m(45) = -1.1970645248657706787857730846325898673892151885992... \times 10^{-79} \\ w'_m(45) = 4.8015404449363210440157850154984037759705748926074... \times 10^{-79} \end{cases} \quad (45)$$

Comparing with the more accurate solution starting from $r = 55$, the errors of the initial values (45) are obtained as shown by Table 13.

Table 13: Errors of the initial values of case V1.

$r = 45$	w_p	w'_p	w_m	w'_m
— Absolute Error —	2.43×10^{-169}	2.07×10^{-168}	3.89×10^{-192}	3.77×10^{-191}
— Relative Error —	2.30×10^{-113}	6.91×10^{-113}	3.25×10^{-113}	7.85×10^{-113}

Numerically integrating (25) from $r = 45$ to $r = 1$ by the Gauss-Legendre method with the same parameters as the ones in Subsection 3.2, the values of w_p , w'_p , w_m and w'_m at $r = 1$ are obtained

$$\begin{cases} w_p(1) = -7.5811708202722819337886291345224915096864160866088... \times 10^{-2} \\ w'_p(1) = 2.4764894905832982616275785124301997778251205645956... \times 10^{-1} \\ w_m(1) = -1.8985818420083245736824441481547286887104902789335... \times 10^{-2} \\ w'_m(1) = 8.0472024534463364925338502074404317836916130555680.... \times 10^{-2} \end{cases} \quad (46)$$

Comparing with the more accurate solution starting from $r = 55$, the errors of (46) are obtained as shown by Table 14.

3.6.2 Near $r = 0$

Near $r = 0$, the transformation is still (31). Hence, the differential equations for \tilde{w}_0 and \tilde{w}_1 are also (32).

Table 14: Errors of the numerical solution at $r = 1$ of case V1.

$r = 1$	w_p	w'_p	w_m	w'_m
— Absolute Error —	3.47×10^{-114}	1.12×10^{-113}	9.71×10^{-115}	3.94×10^{-114}
— Relative Error —	4.58×10^{-113}	4.54×10^{-113}	5.11×10^{-113}	4.89×10^{-113}

Now, $(\gamma_0, \gamma_1) = (3, 1)$ and the expected \tilde{w}_0 and \tilde{w}_1 are of order $o(s)$. So the associated truncation of (32) near $s = -\infty$ for the V1 case is

$$\begin{cases} \frac{1}{4} \frac{d^2 \tilde{w}_0^{(0)}}{ds^2} = -e^{\tilde{w}_1^{(0)} - \tilde{w}_0^{(0)}} \\ \frac{1}{4} \frac{d^2 \tilde{w}_p^{(0)}}{ds^2} = e^{\tilde{w}_1^{(0)} - \tilde{w}_0^{(0)}} - e^{-2\tilde{w}_1^{(0)}} \end{cases} \quad (47)$$

Let

$$\tilde{w}_p^{(0)} = w_0^{(0)} + w_1^{(0)}.$$

Then, we have

$$\begin{cases} \frac{1}{4} \frac{d^2 \tilde{w}_0^{(0)}}{ds^2} = -e^{\tilde{w}_p^{(0)} - 2\tilde{w}_0^{(0)}} \\ \frac{1}{4} \frac{d^2 \tilde{w}_p^{(0)}}{ds^2} = -e^{-2\tilde{w}_p^{(0)} + 2\tilde{w}_0^{(0)}} \end{cases} \quad (48)$$

Unlike the cases discussed before, we have not achieved the general solution of (48). Anyhow, Equation (48) itself deserves an independent investigation. Let us leave it as a future work. Surprisingly, a two parameter family of explicit solutions of (48) can be constructed and the asymptotic solution near $r = 0$ is just among them! By the hint of the asymptotic solution and for the convenience of comparison, we seek the solutions of (48) of form

$$\begin{cases} \tilde{w}_0^{(0)} = \ln(\tilde{a}_3(s - \ln 4)^3 + \tilde{a}_2(s - \ln 4)^2 + \tilde{a}_1(s - \ln 4) + \tilde{a}_0) \\ \tilde{w}_p^{(0)} = \ln(\tilde{b}_4(s - \ln 4)^4 + \tilde{b}_3(s - \ln 4)^3 + \tilde{b}_2(s - \ln 4)^2 + \tilde{b}_1(s - \ln 4) + \tilde{b}_0) \end{cases}.$$

There are only two sets of solutions that has form (49).

Set A:

$$\begin{aligned} \tilde{a}_3 &= \frac{4}{3}, \quad \tilde{b}_4 = \frac{4}{3}, \\ \tilde{a}_1 &= \frac{1}{4}\tilde{a}_2^2, \quad \tilde{b}_3 = \frac{4}{3}\tilde{a}_2, \quad \tilde{b}_2 = \frac{1}{2}\tilde{a}_2^2, \\ \tilde{b}_1 &= \frac{1}{8}(\tilde{a}_2^3 - 16\tilde{a}_0), \quad \tilde{b}_0 = \frac{1}{64}(\tilde{a}_2^4 - 32\tilde{a}_0\tilde{a}_2). \end{aligned}$$

Set B:

$$\begin{aligned} \tilde{a}_3 &= -\frac{4}{3}, \quad \tilde{b}_4 = \frac{4}{3}, \\ \tilde{a}_1 &= -\frac{1}{4}\tilde{a}_2^2, \quad \tilde{b}_3 = -\frac{4}{3}\tilde{a}_2, \quad \tilde{b}_2 = \frac{1}{2}\tilde{a}_2^2, \\ \tilde{b}_1 &= \frac{1}{8}(16\tilde{a}_0 - \tilde{a}_2^3), \quad \tilde{b}_0 = \frac{1}{64}(\tilde{a}_2^4 - 32\tilde{a}_0\tilde{a}_2). \end{aligned}$$

The asymptotic solution is in Set B with

$$\begin{aligned} \tilde{a}_2 &= -4\gamma_{eu}, \\ \tilde{a}_0 &= -\frac{1}{24}\zeta(3) - \frac{4}{3}\gamma_{eu}^3. \end{aligned}$$

The error of the truncation from (32) to (47) is caused by the term $e^{2\tilde{w}_0+8s}$, which is of order $O(s^6 e^{8s})$. So we set $s_f = -32$ since $(-32)^6 e^{8 \times (-32)} \approx 7.1 \times 10^{-103}$ has been smaller than 10^{-100} .

The high-precision numerical solution is obtained by numerically integrating (32) by the Gauss-Legendre method. Comparing it with the more accurate numerical solution starting from $r = 55$, the errors of the numerical solution are obtained. Table 15 shows that our numerical solution is as accurate as we expected.

Table 16 shows how good the asymptotic solution (19) is. Table 16 not only numerically verifies the asymptotics of the V1 case, but also confirms our estimate that \tilde{w}_0 and $\tilde{w}_1 + \tilde{w}_0$ differ from their asymptotics by an order of $O(s^6 e^{8s})$.

Table 15: Errors of the numerical solution at $s = -32$ for the V1 case.

$s = -32$	\tilde{w}_0	$\frac{d\tilde{w}_0}{ds}$	\tilde{w}_1	$\frac{d\tilde{w}_1}{ds}$
— Absolute Error —	1.14×10^{-109}	1.49×10^{-110}	3.94×10^{-109}	4.77×10^{-110}
— Relative Error —	1.06×10^{-110}	1.62×10^{-109}	1.13×10^{-109}	1.57×10^{-108}

Table 16: Approximate derivation from the asymptotic solution for the V1 case.

s	-7	-12	-17	-22	-27	-32
$\ln(\tilde{w}_0 - \ln(P_3))$	-45.6682	-82.7772	-120.834	-159.368	-198.191	-237.207
$\ln(\tilde{w}_0 + \tilde{w}_1 - \ln(P_4))$	-45.6691	-82.7775	-120.834	-159.368	-198.191	-237.207

3.7 Case V2

In this case $(\gamma_0, \gamma_1) = (-1, 1)$.

By the connection formula (10), we have $(s_1^{\mathbb{R}}, s_2^{\mathbb{R}}) = (0, 2)$. $s_1^{\mathbb{R}} = 0$ means $w_1 = -w_0$ at $r = \infty$. This leads to $w_1 \equiv -w_0$ for $r \in (0, \infty)$, considering that they satisfy (7).

Let

$$w = w_0 = -w_1.$$

Then, the differential equation for w is

$$\frac{1}{2} \left(\frac{d^2}{dr^2} + \frac{1}{r} \frac{d}{dr} \right) w = e^{4w} - e^{-4w},$$

which is the radical reduction of the sinh-Gordon equation. Both the associated truncation

$$\frac{1}{4} \frac{d^2 \tilde{w}^{(0)}}{ds^2} = e^{2\tilde{w}^{(0)}} \quad (49)$$

and the numerical experiments show that $2w(r)$ differs from its asymptotics by an order of $O(s^2 e^{4s})$ near $r = 0$.

3.8 Case V3

In this case, $(\gamma_0, \gamma_1) = (-1, -3)$. Thus, $(s_1^{\mathbb{R}}, s_2^{\mathbb{R}}) = (-4, -6)$ by (10). As explained in the beginning of Section 3, the fine asymptotics of the V3 case can be obtained from the V1 case. So we omit the verification.

4 Out of the curved triangle: generalizing the connection formula and the fine asymptotics

First, let us divide the real plane of $(s_1^{\mathbb{R}}, s_2^{\mathbb{R}})$ into 19 parts: regions $\Omega_0, \Omega_1, \Omega_2, \Omega_3, \Omega_4, \Omega_5, \Omega_6$; edges E1, E2, E3, $E_1^U, E_2^U, E_1^D, E_2^D, E_3^R, E_3^L$; and vertices V1, V2, V3. See Figure 3 for details. Note that the boundaries of Ω_i are line $s_2^{\mathbb{R}} = 2s_1^{\mathbb{R}} + 2$, line $s_2^{\mathbb{R}} = -2s_1^{\mathbb{R}} + 2$ and parabola $s_2^{\mathbb{R}} = -\frac{1}{4}(s_1^{\mathbb{R}})^2 - 2$.

By the connection formula (10) (see also Figure 2), on the Stokes data side, the solutions studied in Theorem (1.1) are those parameterized by the point in the region Ω_0 , on the edges E1, E2, E3, and the vertices V1, V2, V3. These solutions are all smooth for $r \in (0, \infty)$. Consider the case where $(s_1^{\mathbb{R}}, s_2^{\mathbb{R}})$ lies outside the curved triangle. Then the corresponding $w_0(r)$, $w_1(r)$, or both must evolve to a singularity somewhere as r decreases from $r = \infty$. Numerical experiments show that there is a cut around every singularity. But we have evidence that these singularities and cuts are artificial: They can be avoided by choosing appropriate variables. For example, if we use variables $v_0 = e^{2w_0}$ and $v_1 = e^{2w_1}$, then v_0 and v_1 will have no cuts near $r > 0$. v_0 or v_1 may still have singularities, i.e., in general, v_0 and v_1 are not the final smooth variables. Fortunately, we were able to find two smooth variables for each part of Figure 3, see Conjecture 4.1. From this point of view, Theorem (1.1) studies only those solutions that have “positivity” property so that they are still real after taking logarithm.

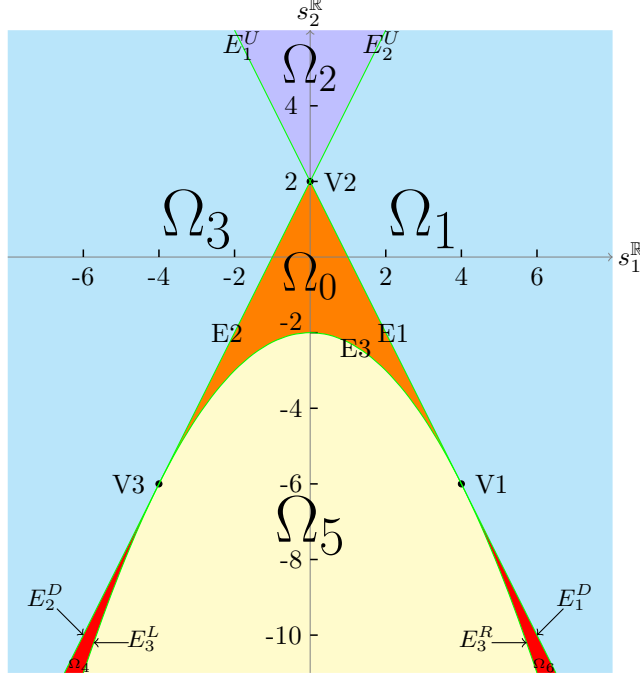


Figure 3: Regions of Ω_i , $i = 0, 1, 2, 3, 4, 5, 6$, edges of $E_1, E_2, E_3, E_1^U, E_2^U, E_1^D, E_2^D, E_3^L, E_3^R$, and vertex of V_1, V_2, V_3 .

4.1 The conjecture

The fine asymptotics for the cases of $\Omega_0, E_1, E_2, E_3, V_1, V_2$ and V_3 have been rigorously proved in [7] and numerically verified in Section 3. So the following conjecture only deals with the other remaining 12 cases: $\Omega_1, \Omega_2, \Omega_3, \Omega_4, \Omega_5, \Omega_6, E_1^U, E_2^U, E_1^D, E_2^D, E_3^R$ and E_3^L . Similar to the explanation at the beginning of Section 3, the formulas of $\Omega_3, \Omega_4, E_1^U, E_2^D$ and E_3^L are symmetrical to those of $\Omega_1, \Omega_6, E_2^U, E_1^D$ and E_3^R , respectively. But for convenience, we will list all formulas for the 12 cases.

Conjecture 4.1. *Let the inverse of connection formula (10) be*

$$\begin{cases} \gamma_0 = \frac{4}{\pi} \arccos \left(-\frac{1}{4}s_1^{\mathbb{R}} + \frac{1}{4}\sqrt{8 + (s_1^{\mathbb{R}})^2 + 4s_2^{\mathbb{R}}} \right) - 1 \\ \gamma_1 = \frac{4}{\pi} \arccos \left(-\frac{1}{4}s_1^{\mathbb{R}} - \frac{1}{4}\sqrt{8 + (s_1^{\mathbb{R}})^2 + 4s_2^{\mathbb{R}}} \right) - 3 \end{cases}, \quad (50)$$

where the values of the arccos terms may be complex and should be given by their principal values. Suppose that $w_0(r)$ and $w_1(r)$ have asymptotic (9) at $r = \infty$ and that (γ_0, γ_1) is calculated from (50). Define (ρ_0, ρ_1) by (14) and $s = \ln(r)$. Denote $\gamma_i^{\mathbb{R}} = \Re(\gamma_i)$, $\gamma_i^{\mathbb{I}} = \Im(\gamma_i)$, $\rho_i^{\mathbb{R}} = \Re(\rho_i)$, $\rho_i^{\mathbb{I}} = \Im(\rho_i)$, $i = 0, 1$. Then, the characteristics of a solution parameterized by a point in region Ω_i , $i = 1, \dots, 6$, are the following.

Ω_1 : $\sqrt{8 + (s_1^{\mathbb{R}})^2 + 4s_2^{\mathbb{R}}} \in \mathbb{R}$, $\gamma_0 \in \mathbb{R}$, $\gamma_1 \notin \mathbb{R}$. $e^{2w_0(r)}$ and $e^{2w_1(r)}$ are smooth for $r \in (0, \infty)$. Their asymptotics at $s = -\infty$ are

$$\begin{cases} e^{2w_0} \xrightarrow{s \rightarrow -\infty} e^{\gamma_0 s + \rho_0} \\ e^{2w_1} \xrightarrow{s \rightarrow -\infty} 2 \Re(e^{\gamma_1 s + \rho_1}) \end{cases}.$$

Ω_2 : $\sqrt{8 + (s_1^{\mathbb{R}})^2 + 4s_2^{\mathbb{R}}} \in \mathbb{R}$, $\gamma_0 \notin \mathbb{R}$, $\gamma_1 \notin \mathbb{R}$. $e^{-2w_0(r)}$ and $e^{2w_1(r)}$ are smooth for $r \in (0, \infty)$. Their asymptotics at $s = -\infty$ are

$$\begin{cases} e^{-2w_0} \xrightarrow{s \rightarrow -\infty} 2 \Re(e^{-\gamma_0 s - \rho_0}) \\ e^{2w_1} \xrightarrow{s \rightarrow -\infty} 2 \Re(e^{\gamma_1 s + \rho_1}) \end{cases}.$$

Ω_3 : $\sqrt{8 + (s_1^{\mathbb{R}})^2 + 4s_2^{\mathbb{R}}} \in \mathbb{R}$, $\gamma_0 \notin \mathbb{R}$, $\gamma_1 \in \mathbb{R}$. $e^{-2w_0(r)}$ and $e^{-2w_1(r)}$ are smooth for $r \in (0, \infty)$. Their asymptotics at $s = -\infty$ are

$$\begin{cases} e^{-2w_0} \xrightarrow{s \rightarrow -\infty} 2 \Re(e^{-\gamma_0 s - \rho_0}) \\ e^{-2w_1} \xrightarrow{s \rightarrow -\infty} e^{-\gamma_1 s - \rho_1} \end{cases}.$$

$\Omega_4 : \sqrt{8 + (s_1^{\mathbb{R}})^2 + 4s_2^{\mathbb{R}}} \in \mathbb{R}$, $\gamma_0 \notin \mathbb{R}$, $\gamma_1 \notin \mathbb{R}$. $e^{-2w_1(r)}$ and $e^{-2w_0(r)-2w_1(r)}$ are smooth for $r \in (0, \infty)$. Their asymptotics at $s = -\infty$ are

$$\left\{ \begin{array}{ll} e^{-2w_1} & \xrightarrow{s \rightarrow -\infty} e^{-\gamma_1^{\mathbb{R}} s} \left(\frac{8e^{-\rho_0^{\mathbb{R}}}}{(\gamma_0^{\mathbb{I}} - \gamma_1^{\mathbb{I}})^2} \cos(\gamma_0^{\mathbb{I}} s + \rho_0^{\mathbb{I}}) + 2e^{-\rho_1^{\mathbb{R}}} \cos(\gamma_1^{\mathbb{I}} s + \rho_1^{\mathbb{I}}) \right) \\ e^{-2w_0-2w_1} & \xrightarrow{s \rightarrow -\infty} e^{-(\gamma_0^{\mathbb{R}} + \gamma_1^{\mathbb{R}})s} \left\{ 2e^{-\rho_0^{\mathbb{R}} - \rho_1^{\mathbb{R}}} \frac{(\gamma_0^{\mathbb{I}} + \gamma_1^{\mathbb{I}})^2}{(\gamma_0^{\mathbb{I}} - \gamma_1^{\mathbb{I}})^2} \cos((\gamma_0^{\mathbb{I}} - \gamma_1^{\mathbb{I}})s + \rho_0^{\mathbb{I}} - \rho_1^{\mathbb{I}}) \right. \\ & \left. + \frac{16e^{-2\rho_0^{\mathbb{R}}}(\gamma_0^{\mathbb{I}})^2}{(\gamma_0^{\mathbb{I}} - \gamma_1^{\mathbb{I}})^4} + e^{-2\rho_1^{\mathbb{R}}}(\gamma_1^{\mathbb{I}})^2 + 2e^{-\rho_0^{\mathbb{R}} - \rho_1^{\mathbb{R}}} \cos((\gamma_0^{\mathbb{R}} + \gamma_1^{\mathbb{R}})s + \rho_0^{\mathbb{I}} + \rho_1^{\mathbb{I}}) \right\} \end{array} \right.$$

$\Omega_5 : \sqrt{8 + (s_1^{\mathbb{R}})^2 + 4s_2^{\mathbb{R}}} \notin \mathbb{R}$, $\gamma_0 \notin \mathbb{R}$, $\gamma_1 \notin \mathbb{R}$. $e^{2w_0(r)}$ and $e^{-2w_1(r)}$ are smooth for $r \in (0, \infty)$. Their asymptotics at $s = -\infty$ are

$$\left\{ \begin{array}{ll} e^{2w_0} & \xrightarrow{s \rightarrow -\infty} 2\Re(e^{\gamma_0 s + \rho_0}) \\ e^{-2w_1} & \xrightarrow{s \rightarrow -\infty} 2\Re(e^{-\gamma_1 s - \rho_1}) \end{array} \right.$$

$\Omega_6 : \sqrt{8 + (s_1^{\mathbb{R}})^2 + 4s_2^{\mathbb{R}}} \in \mathbb{R}$, $\gamma_0 \notin \mathbb{R}$, $\gamma_1 \notin \mathbb{R}$. $e^{2w_0(r)}$ and $e^{2w_0(r)+2w_1(r)}$ are smooth for $r \in (0, \infty)$. Their asymptotics at $s = -\infty$ are

$$\left\{ \begin{array}{ll} e^{2w_0} & \xrightarrow{s \rightarrow -\infty} e^{\gamma_0^{\mathbb{R}} s} \left(\frac{8e^{\rho_1^{\mathbb{R}}}}{(\gamma_0^{\mathbb{I}} - \gamma_1^{\mathbb{I}})^2} \cos(\gamma_1^{\mathbb{I}} s + \rho_1^{\mathbb{I}}) + 2e^{\rho_0^{\mathbb{R}}} \cos(\gamma_0^{\mathbb{I}} s + \rho_0^{\mathbb{I}}) \right) \\ e^{2w_0+2w_1} & \xrightarrow{s \rightarrow -\infty} e^{(\gamma_0^{\mathbb{R}} + \gamma_1^{\mathbb{R}})s} \left\{ 2e^{\rho_0^{\mathbb{R}} + \rho_1^{\mathbb{R}}} \frac{(\gamma_0^{\mathbb{I}} + \gamma_1^{\mathbb{I}})^2}{(\gamma_0^{\mathbb{I}} - \gamma_1^{\mathbb{I}})^2} \cos((\gamma_0^{\mathbb{I}} - \gamma_1^{\mathbb{I}})s + \rho_0^{\mathbb{I}} - \rho_1^{\mathbb{I}}) \right. \\ & \left. + \frac{16e^{2\rho_1^{\mathbb{R}}}(\gamma_1^{\mathbb{I}})^2}{(\gamma_0^{\mathbb{I}} - \gamma_1^{\mathbb{I}})^4} + e^{2\rho_0^{\mathbb{R}}}(\gamma_0^{\mathbb{I}})^2 + 2e^{\rho_0^{\mathbb{R}} + \rho_1^{\mathbb{R}}} \cos((\gamma_0^{\mathbb{R}} + \gamma_1^{\mathbb{R}})s + \rho_0^{\mathbb{I}} + \rho_1^{\mathbb{I}}) \right\} \end{array} \right.$$

On the edges, $8 + (s_1^{\mathbb{R}})^2 + 4s_2^{\mathbb{R}}$ is always non-negative. Define

$$\begin{aligned} b_1 &= \frac{1}{2}\psi\left(\frac{3-\gamma_0}{8}\right) + \frac{1}{2}\psi\left(\frac{5+\gamma_0}{8}\right) - \gamma_{eu} + 4\ln 2, \\ b_2 &= \frac{1}{2}\psi\left(\frac{3+\gamma_1}{8}\right) + \frac{1}{2}\psi\left(\frac{5-\gamma_1}{8}\right) - \gamma_{eu} + 4\ln 2, \\ b_3 &= -\frac{1}{4}\psi\left(\frac{3-\gamma_0}{4}\right) - \frac{1}{4}\psi\left(\frac{\gamma_0-3}{4}\right) + \frac{1}{3-\gamma_0} - 2\ln 2 + \frac{\gamma_{eu}}{2}. \end{aligned}$$

Then, the characteristics of a solution parameterized by a point on an edge are the following.

$E_1^U : \gamma_0 \notin \mathbb{R}$, $\gamma_1 = 1$, $\gamma_0^{\mathbb{R}} = -1$, $\rho_0 \notin \mathbb{R}$ and ρ_1 is not defined. $e^{-2w_0(r)}$ and $e^{2w_1(r)}$ are smooth for $r \in (0, \infty)$. Their asymptotics at $s = -\infty$ are

$$\left\{ \begin{array}{ll} e^{-2w_0} & \xrightarrow{s \rightarrow -\infty} 2\Re(e^{-\gamma_0 s - \rho_0}) \\ e^{2w_1(r)} & \xrightarrow{s \rightarrow -\infty} -2s + b_1 \end{array} \right.$$

$E_2^U : \gamma_0 = -1$, $\gamma_1 \notin \mathbb{R}$, $\gamma_1^{\mathbb{R}} = 1$, $\rho_1 \notin \mathbb{R}$ and ρ_0 is not defined. $e^{-2w_0(r)}$ and $e^{2w_1(r)}$ are smooth for $r \in (0, \infty)$. Their asymptotics at $s = -\infty$ are

$$\left\{ \begin{array}{ll} e^{-2w_0} & \xrightarrow{s \rightarrow -\infty} -2s + b_2 \\ e^{2w_1(r)} & \xrightarrow{s \rightarrow -\infty} 2\Re(e^{\gamma_1 s + \rho_1}) \end{array} \right.$$

$E_1^D : \gamma_0 = 3$, $\gamma_1 \notin \mathbb{R}$, $\gamma_1^{\mathbb{R}} = 1$, $\rho_1 \notin \mathbb{R}$ and ρ_0 is not defined. $e^{2w_1(r)}$ and $e^{2w_0(r)}$ are smooth for $r \in (0, \infty)$. Their asymptotics at $s = -\infty$ are

$$\left\{ \begin{array}{ll} e^{2w_0(r)} & \xrightarrow{s \rightarrow -\infty} e^{\gamma_0 s} \left(-\frac{8}{(\gamma_1^{\mathbb{I}})^2} s + d_0 - \frac{8}{(\gamma_1^{\mathbb{I}})^3} \cos(\gamma_1^{\mathbb{I}} s + \rho_1^{\mathbb{I}}) \right) \\ e^{2w_1} & \xrightarrow{s \rightarrow -\infty} 2e^{\gamma_1^{\mathbb{R}} s + \rho_1^{\mathbb{R}}} \left(\cos(\gamma_1^{\mathbb{I}} s + \rho_1^{\mathbb{I}}) + \frac{(1 - \sin(\gamma_1^{\mathbb{I}} s + \rho_1^{\mathbb{I}}))^2}{\gamma_1^{\mathbb{I}} s - \frac{(\gamma_1^{\mathbb{I}})^3}{8} d_0 + \cos(\gamma_1^{\mathbb{I}} s + \rho_1^{\mathbb{I}})} \right) \end{array} \right.,$$

where $d_0 = \lim_{s_1^{\mathbb{R}} \rightarrow 1 - \frac{s_2^{\mathbb{R}}}{2} + 0_-} 2e^{\rho_0^{\mathbb{R}}}(\rho_0^{\mathbb{I}} + \frac{\pi}{2})$.

$E_2^D : \gamma_0 \notin \mathbb{R}, \gamma_1 = -3, \gamma_0^{\mathbb{R}} = -1, \rho_0 \notin \mathbb{R}$ and ρ_1 is not defined. $e^{-2w_0(r)}$ and $e^{-2w_1(r)}$ are smooth for $r \in (0, \infty)$. Their asymptotics at $s = -\infty$ are

$$\begin{cases} e^{-2w_0} \xrightarrow{s \rightarrow -\infty} 2 e^{-\gamma_0^{\mathbb{R}} s - \rho_0^{\mathbb{R}}} \left(\cos(\gamma_0^{\mathbb{I}} s + \rho_0^{\mathbb{I}}) + \frac{8(1 + \sin(\gamma_0^{\mathbb{I}} s + \rho_0^{\mathbb{I}}))^2}{-8\gamma_0^{\mathbb{I}} s + (\gamma_0^{\mathbb{I}})^3 \tilde{d}_0 + 8 \cos(\gamma_0^{\mathbb{I}} s + \rho_0^{\mathbb{I}})} \right) \\ e^{-2w_1(r)} \xrightarrow{s \rightarrow -\infty} e^{-\gamma_1 s} \left(-\frac{8}{(\gamma_0^{\mathbb{I}})^2} s + \tilde{d}_0 + \frac{8}{(\gamma_0^{\mathbb{I}})^3} \cos(\gamma_0^{\mathbb{I}} s + \rho_0^{\mathbb{I}}) \right) \end{cases},$$

where $\tilde{d}_0 = \lim_{s_1^{\mathbb{R}} \rightarrow \frac{s_2^{\mathbb{R}}}{2} - 1 + 0_+} 2 e^{-\rho_1^{\mathbb{R}}} \left(\frac{\pi}{2} - \rho_1^{\mathbb{I}} \right).$

$E_3^R : \gamma_0 \notin \mathbb{R}, \gamma_1 \notin \mathbb{R}, \gamma_0^{\mathbb{R}} = 3, \gamma_1^{\mathbb{R}} = 1$ and $\gamma_0^{\mathbb{I}} = \gamma_1^{\mathbb{I}}$. Both ρ_0 and ρ_1 are not defined. $e^{2w_0(r)}$ and $e^{2w_0(r)+2w_1(r)}$ are smooth for $r \in (0, \infty)$. Their asymptotics at $s = -\infty$ are

$$\begin{cases} e^{2w_0} \xrightarrow{s \rightarrow -\infty} -e^{\gamma_0^{\mathbb{R}} s} \left(\frac{4}{(\gamma_0^{\mathbb{I}})^2} (s + \Re(b_3)) \sin(\gamma_0^{\mathbb{I}} s + \theta_0) + \frac{4}{(\gamma_0^{\mathbb{I}})^3} \cos(\gamma_0^{\mathbb{I}} s + \theta_0) \right) \\ e^{2w_0+2w_1(r)} \xrightarrow{s \rightarrow -\infty} e^{(\gamma_0^{\mathbb{R}} + \gamma_1^{\mathbb{R}}) s} \left(\frac{4}{(\gamma_0^{\mathbb{I}})^2} (s + \Re(b_3))^2 - \frac{4}{(\gamma_0^{\mathbb{I}})^4} (\cos(\gamma_0^{\mathbb{I}} s + \theta_0))^2 \right) \end{cases},$$

where $\theta_0 = \lim_{s_1^{\mathbb{R}} \rightarrow 2\sqrt{-2-s_2^{\mathbb{R}}}+0_+} \rho_0^{\mathbb{I}}.$

$E_3^L : \gamma_0 \notin \mathbb{R}, \gamma_1 \notin \mathbb{R}, \gamma_0^{\mathbb{R}} = -1, \gamma_1^{\mathbb{R}} = -3$ and $\gamma_0^{\mathbb{I}} = \gamma_1^{\mathbb{I}}$. Both ρ_0 and ρ_1 are not defined. $e^{-2w_1(r)}$ and $e^{-2w_0(r)-2w_1(r)}$ are smooth for $r \in (0, \infty)$. Their asymptotics at $s = -\infty$ are

$$\begin{cases} e^{-2w_1} \xrightarrow{s \rightarrow -\infty} e^{-\gamma_1^{\mathbb{R}} s} \left(\frac{4}{(\gamma_1^{\mathbb{I}})^2} (s + \Re(b_3)) \sin(\gamma_1^{\mathbb{I}} s - \tilde{\theta}_0) + \frac{4}{(\gamma_1^{\mathbb{I}})^3} \cos(\gamma_1^{\mathbb{I}} s - \tilde{\theta}_0) \right) \\ e^{-2w_0-2w_1(r)} \xrightarrow{s \rightarrow -\infty} e^{-(\gamma_0^{\mathbb{R}} + \gamma_1^{\mathbb{R}}) s} \left(\frac{4}{(\gamma_1^{\mathbb{I}})^2} (s + \Re(b_3))^2 - \frac{4}{(\gamma_1^{\mathbb{I}})^4} (\cos(\gamma_1^{\mathbb{I}} s - \tilde{\theta}_0))^2 \right) \end{cases},$$

where $\tilde{\theta}_0 = - \lim_{s_1^{\mathbb{R}} \rightarrow -2\sqrt{-2-s_2^{\mathbb{R}}}+0_-} \rho_1^{\mathbb{I}}.$

4.2 Numerically verify the conjecture: the Ω_1 case as an example

In this subsection, we will numerically verify Conjecture 4.1 for the Ω_1 case with $(s_1^{\mathbb{R}}, s_2^{\mathbb{R}}) = (2, 1)$. Then by (50) we get

$$\begin{cases} \gamma_0|_{s_1^{\mathbb{R}}=2, s_2^{\mathbb{R}}=1} = \frac{1}{3} \\ \gamma_1|_{s_1^{\mathbb{R}}=2, s_2^{\mathbb{R}}=1} = \frac{4}{\pi} \arccos(-\frac{3}{2}) - 3 = 1 + \frac{4i}{\pi} \ln(\frac{3-\sqrt{5}}{2}) \end{cases}. \quad (51)$$

With $(s_1^{\mathbb{R}}, s_2^{\mathbb{R}}) = (2, 1)$, w_0 and w_1 keep real as r decreasing from $r = \infty$ to $r = 1$. So we do not need adjust our numerical integration for $r > 1$.

By the truncation of (27), the initial values at $r = 45$ are obtained (only the first 50 digits are listed)

$$\begin{cases} w_p(45) = -5.2843098725232974899221393911204991207504443469367... \times 10^{-57} \\ w'_p(45) = 1.5004885502015739552694025310567337731833237644509... \times 10^{-56} \\ w_m(45) = 1.9951075414429511313096218077209854214432475688359... \times 10^{-80} \\ w'_m(45) = -8.0025674082272017400263083591640194065100562879396... \times 10^{-80} \end{cases}. \quad (52)$$

Comparing with the more accurate solution starting from $r = 55$, the errors of the initial values (52) are obtained as shown by Table 17.

Table 17: Errors of the initial values of case Ω_1 with $(s_1^{\mathbb{R}}, s_2^{\mathbb{R}}) = (2, 1)$.

$r = 45$	w_p	w'_p	w_m	w'_m
— Absolute Error —	3.04×10^{-170}	2.59×10^{-169}	1.62×10^{-193}	1.57×10^{-192}
— Relative Error —	5.76×10^{-114}	1.73×10^{-113}	8.12×10^{-114}	1.96×10^{-113}

Numerically integrating (25) from $r = 45$ to $r = 1$ by the Gauss-Legendre method with parameters as same as the ones used in Subsection 3.2, the values of w_p , w'_p , w_m and w'_m at $r = 1$ are obtained

$$\begin{cases} w_p(1) = -3.8224055163443861381648888321249635590437848425393... \times 10^{-2} \\ w'_p(1) = 1.2620798170393397054252193737795545512207073701669... \times 10^{-1} \\ w_m(1) = 4.1421810495867924927295926159960489963050832028643... \times 10^{-3} \\ w'_m(1) = -1.9704834137414281607395710259152505912708048802280.... \times 10^{-2} \end{cases}. \quad (53)$$

Table 18: Errors of the numerical solution at $r = 1$ of case Ω_1 with $(s_1^{\mathbb{R}}, s_2^{\mathbb{R}}) = (2, 1)$.

$r = 1$	w_p	w'_p	w_m	w'_m
— Absolute Error —	4.42×10^{-115}	1.46×10^{-114}	6.30×10^{-116}	3.09×10^{-115}
— Relative Error —	1.16×10^{-113}	1.16×10^{-113}	1.52×10^{-113}	1.57×10^{-113}

Comparing with the more accurate solution starting from $r = 55$, the errors of (46) are obtained as shown by Table 18.

When $r < 1$, w_0 and w_1 may be complex. As Conjecture 4.1 suggests, we use v_0 and v_1

$$\begin{cases} v_0 = e^{2w_0} \\ v_1 = e^{2w_1} \end{cases} \quad (54)$$

as dependent variables for the Ω_1 case. Then, v_0 and v_1 will be real for $r > 0$.

To improve computation efficiency, we use $s = \ln(r)$ as independent variable. Then the equations for v_0 and v_1 are

$$\begin{cases} \frac{d^2 v_0}{ds^2} = 4e^{2s}(v_0^3 - v_1) + \frac{1}{v_0} \left(\frac{dv_0}{ds} \right)^2 \\ \frac{d^2 v_1}{ds^2} = 4e^{2s} \left(\frac{v_1^2}{v_0} - \frac{1}{v_1} \right) + \frac{1}{v_1} \left(\frac{dv_1}{ds} \right)^2 \end{cases} \quad (55)$$

The associated truncation of (55) for the fine asymptotics of the Ω_1 case should be

$$\begin{cases} \frac{d^2 v_0^{(0)}}{ds^2} = \frac{1}{v_0^{(0)}} \left(\frac{dv_0^{(0)}}{ds} \right)^2 \\ \frac{d^2 v_1^{(0)}}{ds^2} = -\frac{4e^{2s}}{v_1^{(0)}} + \frac{1}{v_1^{(0)}} \left(\frac{dv_1^{(0)}}{ds} \right)^2 \end{cases} \quad (56)$$

In fact, after substituting (51) to the Ω_1 case of Conjecture 4.1, it becomes obvious which terms of (55) should be ignored. The solution of (56) is known

$$\begin{cases} v_0^{(0)}(s) = e^{a_{1\Omega_1}s + b_{1\Omega_1}} \\ v_1^{(0)}(s) = -\frac{2}{a_{2\Omega_1}} e^s \cos(a_{2\Omega_1}s + b_{2\Omega_1}) \end{cases} \quad (57)$$

Comparing (57) with Conjecture 4.1, we know that $a_{1\Omega_1} = \gamma_0$, $b_{1\Omega_1} = \rho_0$, $a_{2\Omega_1} = \Im(\gamma_1)$ and $b_{2\Omega_1} = \Im(\rho_1)$. Note also that $-\frac{1}{\Im(\gamma_1)} = e^{\Re(\rho_1)}$ in the Ω_1 case. The ignored terms of the truncation from (55) to (56) are $4e^{2s}(v_0^3 - v_1)$ and $4e^{2s}\frac{v_1^2}{v_0}$, which, considering (51), are of order $O(e^{3s})$ and $O(e^{\frac{11}{3}s})$, respectively. So the relative errors are both of order $O(e^{\frac{8}{3}s})$ except near the zeros of $v_1(s)$. Since v_0 and v_1 are both small in this case, only the relative errors are relevant. To avoid the inconvenience brought by the relative error, we will take

$$\begin{cases} \Delta_0(s) = |e^{2w_0} e^{-\gamma_0 s - \rho_0} - 1| \\ \Delta_1(s) = |\frac{1}{2} e^{2w_1} e^{-\Re(\gamma_1)s - \Re(\rho_1)} - \cos(\Im(\gamma_1)s + \Im(\rho_1))| \end{cases} \quad (58)$$

as the measurement of error. So Δ_0 and Δ_1 are both of order $O(e^{\frac{8}{3}s})$. Solving $e^{\frac{8}{3}s_f} = 10^{-100}$, we get $s_f \approx -86.35$. For safety and convenience, we set $s_f = -87$.

Numerical results show that $v_0(s)$ has no zero for $s \in (-\infty, 0]$ but $v_1(s)$ has, just as Conjecture 4.1 predicts. For the sake of numerical integration, it is better to integrate around the zeros of $v_1(s)$. In order to keep away from the zeros of $v_1(s)$, we first compute $v_0(s + i\epsilon)$ with $\epsilon = 10^{-2}$ to determine the approximate zeros of $v_1(s)$ by solving $\text{Re}(v_1(s + i\epsilon)) = 0$. Then we get the approximate zeros s_i of $v_1(s)$ within the range $-87 \leq s \leq 0$. Table 19 lists the first few of them.

Table 19: The first few approximate zeros s_i of $v_1(s)$ for the Ω_1 case with $(s_1^{\mathbb{R}}, s_2^{\mathbb{R}}) = (2, 1)$.

s_i	s_1	s_2	s_3	s_4	s_5	s_6	s_7	s_8
value	-2.506	-5.069	-7.633	-10.197	-12.760	-15.324	-17.888	-20.452

Obviously, the distance between two adjacent zeros in Table 19 is about 2.5. To avoid the numerical instabilities caused by those zeros, we use a contour in the complex plane of s , as shown in Figure 4.

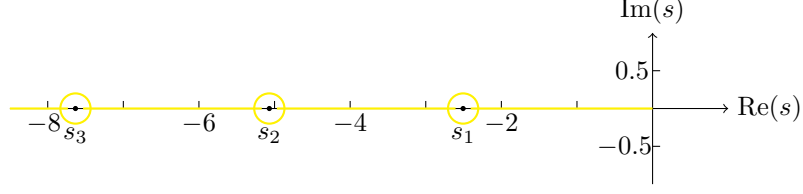


Figure 4: Contour in the complex plane of s to compute $v_0(s)$ and $v_1(s)$.

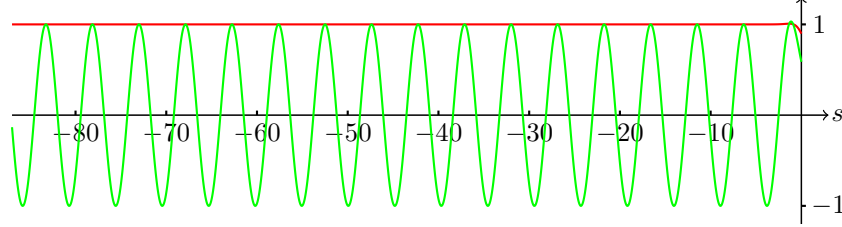


Figure 5: Red, $e^{-\gamma_0 s - \rho_0} v_0(s)$; Green, $\frac{1}{2} e^{-\Re(\gamma_1)s - \Re(\rho_1)} v_1(s)$.

The radii of the circles around the zeros are set to $\frac{1}{5}$. In principle, the values of v_i can be evaluated using the Cauchy integral formula $v_i(s) = \frac{1}{2\pi i} \oint \frac{v_i(\xi)}{\xi - s} d\xi$. But $v_i(\xi)$ has high-precision value only at some fixed points on the circle. At all other points, interpolation must be used, which is not suitable for high-precision purposes. Since v_i are periodic functions on the circle, we use the trapezoidal rule to calculate them

$$v_i(s) = \frac{1}{2n} \sum_j \frac{\tilde{v}_i(\theta_j)}{Re^{i\theta_j} - s} Re^{i\theta_j}, \quad i = 0, 1, \quad (59)$$

where $R = \frac{1}{5}$ denotes the radius of the circle, and $\tilde{v}_i(\theta_j)$ the value of v_i at θ_j on the circle. The distance between the adjacent θ_j is $\frac{\pi}{n}$. Obviously, formula (59) is not appropriate for a point near the circle. Therefore, the contour has 2 line segments in each circle. We use line segments of length $\frac{1}{10}$. In our numerical experiments, n is equal to 1000, which is far more than enough to guarantee an accuracy better than 10^{-100} .

The plots of v_0 and v_1 are shown in Figure 5.

Table 20 shows that the numerical solution is as accurate as we expected.

Table 20: Errors of the numerical solution at $s = -87$ for the Ω_1 case with $(s_1^{\mathbb{R}}, s_2^{\mathbb{R}}) = (2, 1)$.

$s = -87$	v_0	$\frac{dv_0}{ds}$	v_1	$\frac{dv_1}{ds}$
— Absolute Error —	4.06×10^{-125}	1.31×10^{-125}	2.75×10^{-149}	2.30×10^{-149}
— Relative Error —	1.48×10^{-112}	1.43×10^{-112}	7.69×10^{-111}	6.35×10^{-112}

Table 21 shows how good the asymptotic solution is.

5 Deviating from (14)

This section is concerned with what the solution looks like when (14) is not satisfied. First, we derive a better asymptotics near $r = 0$, which is suitable to give initial values for the numerical integration. Then, (7) is integrated numerically. The integration contour on the complex plane of r is used to surround the singularities. We will find that the singularities are regularly distributed. But here we have not been able to derive precise formulas from the limited numerical results. This is very different from the situation in Section 4, where we have formulated a conjecture with substantial formulas based on the numerical results. This is because the difficulties here are much greater than the those encountered in Section 4: Here we have in fact four independent parameters γ_0 , γ_1 , ρ_0 and ρ_1 , while in Section 4 we have essentially only two parameters $s_1^{\mathbb{R}}$ and $s_2^{\mathbb{R}}$.

Table 21: Approximate derivation from the asymptotic solution for the Ω_1 case with $(s_1^{\mathbb{R}}, s_2^{\mathbb{R}}) = (2, 1)$.

s	-27	-37	-47	-57	-67	-77	-87
$\ln(\Delta_0(s))$	-73.2379	-100.773	-130.684	-155.003	-181.988	-208.457	-233.699
$\ln(\Delta_1(s))$	-72.5076	-98.9279	-125.524	-152.287	-179.229	-206.373	-233.697

For convenience, in this section we will always use dependent the variables v_0 and v_1 as defined by (54). As the independent variable, we use $s = \ln(r)$ for $r \leq 1$ as before. So the equations for v_0 and v_1 are still (55).

Let us take the following assumption first.

Assumption 1: Both terms $4e^{2s}(v_0^3 - v_1)$ and $4e^{2s}\left(\frac{v_1^2}{v_0} - \frac{1}{v_1}\right)$ in (55) are negligible near $s = -\infty$.

So (55) becomes

$$\begin{cases} \frac{d^2 v_0^{(0)}}{ds^2} = \frac{1}{v_0^{(0)}} \left(\frac{dv_0^{(0)}}{ds} \right)^2 \\ \frac{d^2 v_1^{(0)}}{ds^2} = \frac{1}{v_1^{(0)}} \left(\frac{dv_1^{(0)}}{ds} \right)^2 \end{cases} \quad (60)$$

The solution of (60) is

$$v_0^{(0)} = c_0 e^{\gamma_0 s}, \quad v_1^{(0)} = c_1 e^{\gamma_1 s}, \quad (61)$$

where c_0, c_1, γ_0 and γ_1 are constants, which should be real if we only interest in the real solutions of (55). The immediate result of Assumption 1 is that γ_0 and γ_1 satisfy the constraints $3\gamma_0 + 2 > \gamma_0$, $\gamma_1 + 2 > \gamma_0$, $2\gamma_1 - \gamma_0 + 2 > \gamma_1$ and $2 - \gamma_1 > \gamma_1$, which is just the inner of the triangle in Figure 2. So, if (γ_0, γ_1) is a point inside the triangle in Figure 2, then $(v_0^{(0)}, v_1^{(0)})$ of (61) is the primary approximate solution of (v_0, v_1) near $s = -\infty$. If $c_0 = e^{\rho_0}$ and $c_1 = e^{\rho_1}$ with ρ_0 and ρ_1 defined by (14), then the solution is the one treated by Theorem 1.1. Here we are interested in the case where $c_0 \neq e^{\rho_0}$ or $c_1 \neq e^{\rho_1}$.

Now, let us transform (55) to its integral form

$$\begin{cases} v_0(s) = c_0 e^{\gamma_0 s} e^{4 \int_{-\infty}^s d\xi \int_{-\infty}^{\xi} d\zeta [v_0(\zeta)^2 - \frac{v_1(\zeta)}{v_0(\zeta)}] e^{2\zeta}} \\ v_1(s) = c_1 e^{\gamma_1 s} e^{4 \int_{-\infty}^s d\xi \int_{-\infty}^{\xi} d\zeta [\frac{v_1(\zeta)}{v_0(\zeta)} - \frac{1}{v_1(\zeta)^2}] e^{2\zeta}} \end{cases} \quad (62)$$

In principle, (62) can be solved recursively near $s = -\infty$: $v_0^{(0)}$ and $v_1^{(0)}$ are given by (61); $v_0^{(1)}$ and $v_1^{(1)}$ are

$$\begin{cases} v_0^{(1)}(s) = c_0 e^{\gamma_0 s} \exp \left\{ \frac{c_0^2}{(1+\gamma_0)^2} e^{2(1+\gamma_0)s} - \frac{4c_1}{c_0(2-\gamma_0+\gamma_1)^2} e^{(2-\gamma_0+\gamma_1)s} \right\} \\ v_1^{(1)}(s) = c_1 e^{\gamma_1 s} \exp \left\{ \frac{4c_1}{c_0(2-\gamma_0+\gamma_1)^2} e^{(2-\gamma_0+\gamma_1)s} - \frac{1}{c_1^2(1-\gamma_1)^2} e^{2(1-\gamma_1)s} \right\} \end{cases}, \quad (63)$$

which are obtained by substituting $v_0 = v_0^{(0)}$ and $v_1 = v_1^{(0)}$ to the right of (62); and so on and so forth. If (γ_0, γ_1) is inside the triangle in Figure 2, then $v_0^{(i)}$ and $v_1^{(i)}$ converge as i increases.

5.1 Numerical solution

As Subsection 3.2, we still use $(\gamma_0, \gamma_1) = (1, \frac{1}{3})$. To have some deviation from Subsection 3.2, c_0 and c_1 should be chosen as

$$c_0 = e^{\rho_0} + \delta c_0, \quad c_1 = e^{\rho_1} + \delta c_1,$$

where δc_0 and δc_1 can not be 0 simultaneously. In the following numerical experiment, we use

$$\delta c_0 = \frac{1}{2}, \quad \delta c_1 = \frac{1}{5}.$$

To solve (55) numerically, the initial values of $(v_0, \frac{dv_0}{ds}, v_1, \frac{dv_1}{ds})$ must be given. We start from $s_1 = -100$ and give the initial values by (63). Since it is easy to compute the initial values by (63), the details of the initial values are omitted. We only list the errors of the initial value by Table 22.

Table 22: Errors of the numerical solution at $s = -100$ with $(\gamma_0, \gamma_1, c_0, c_1) = (1, \frac{1}{3}, e^{\rho_0} + \frac{1}{2}, e^{\rho_1} + \frac{1}{5})$.

$s = -100$	v_0	$\frac{dv_0}{ds}$	v_1	$\frac{dv_1}{ds}$
— Absolute Error —	5.32×10^{-160}	1.95×10^{-159}	2.47×10^{-131}	7.42×10^{-131}
— Relative Error —	4.86×10^{-117}	1.78×10^{-116}	5.12×10^{-117}	4.61×10^{-116}

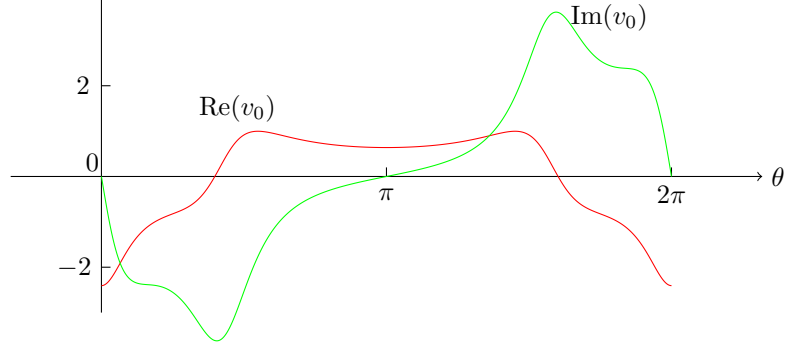


Figure 6: Plots of $v_0(r_1 + R_1 e^{i\theta})$. $r_1 \approx 1.539167317$ is the location of the first singularity and $R_1 \approx 0.239167317$ is the radius of the circle around the singularity.

The errors of the values at $s = -100$ are obtained by comparing them with the numerical solution starting from $s = -140$, which is much more accurate.

The numerical solution is smooth for $s \in [-100, 0]$.

As a comparison to (30), the values of v_0 and others at $s = 0$ are

$$\begin{cases} v_0|_{s=0} = 1.3324864759152155716932764336782719490481063559703... \\ \frac{dv_0}{ds}|_{s=0} = 0.49495834671586092263807187324781656576576424051419... \\ v_1|_{s=0} = 2.6783375094329925626474416219547736732331423595096... \\ \frac{dv_1}{ds}|_{s=0} = 6.2948008049596612397631881197126092308528410458148... \end{cases} \quad (64)$$

Table 23 gives the errors of (64).

Table 23: Errors of the numerical solution at $s = 0$.

$s = 0$	v_0	$\frac{dv_0}{ds}$	v_1	$\frac{dv_1}{ds}$
— Absolute Error —	3.37×10^{-113}	1.69×10^{-112}	5.96×10^{-113}	3.43×10^{-112}
— Relative Error —	2.53×10^{-113}	3.41×10^{-112}	2.23×10^{-113}	5.44×10^{-113}

Again, the errors are evaluated by comparing the two numerical solutions starting from $s = -140$ and from $s = -100$, respectively.

For $s > 0$, i.e. $r > 1$, it is convenient to use the variable r itself instead of s : The pattern of the singularities is more transparent with respect to r than with respect to s . Then (55) is converted to

$$\begin{cases} \frac{dv_0}{dr} = \frac{1}{r} p_0 \\ \frac{dp_0}{dr} = \frac{p_0^2}{rv_0} + 4rv_0^3 - 4rv_1 \\ \frac{dv_1}{dr} = \frac{1}{r} p_1 \\ \frac{dp_1}{dr} = \frac{p_1^2}{rv_1} - \frac{4r}{v_1} + \frac{4rv_1^2}{v_0} \end{cases} \quad (65)$$

Then, we compute the numerical solution of (65), for which the initial values are given by (64). Near $r \approx 1.539167317$, the numerical solution blows up. Figure 6 and 7 show the plots of v_0 and v_1 on the circle with a radius of about 0.239167317 around the singular point.

Obviously, v_0 and v_1 are smooth functions on the circle. Numerical results show that the singularity at $r \approx 1.539167317$ is a simple pole of v_1 . By (65), either $v_0 = \infty$ or $v_0 = 0$ at the singularity of v_1 . Numerical results indicate $v_0 = 0$ at this singularity of v_1 .

To show the pattern of the singularities of v_0 and v_1 , we plot $v_i(r + 10^{-2}i)$, $i = 0, 1$ as Figure 8 and Figure 9.

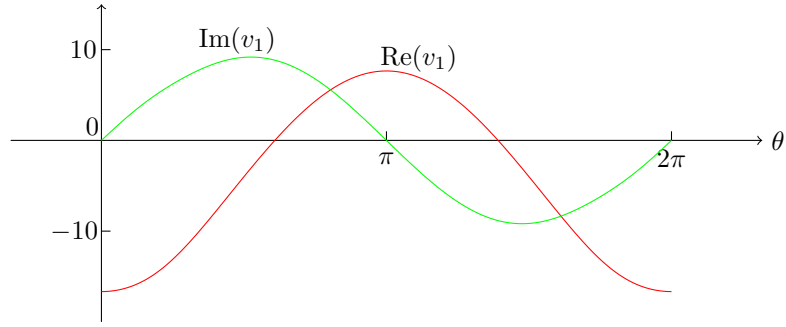


Figure 7: Plots of $v_1(r_1 + R_1 e^{i\theta})$. $r_1 \approx 1.539167317$ is the location of the first singularity and $R_1 \approx 0.239167317$ is the radius of the circle around the singularity.

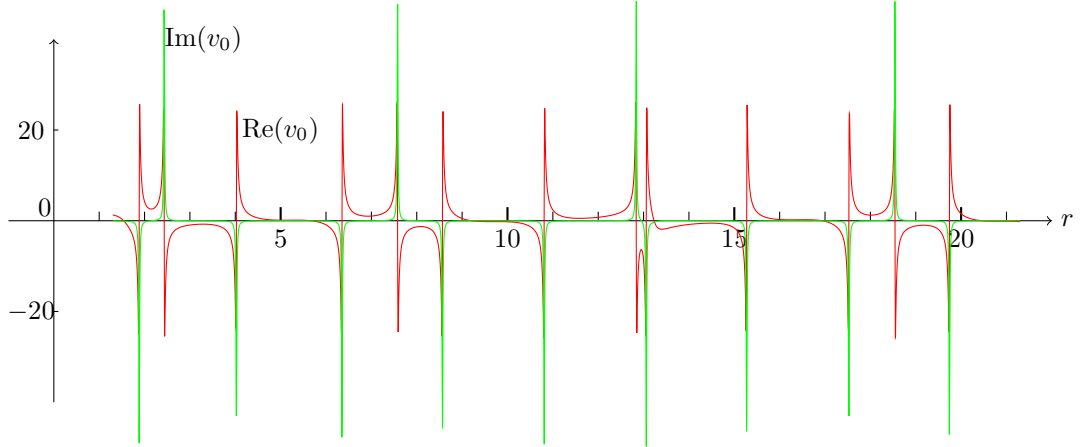


Figure 8: Plot of $v_0(r + 10^{-2}i)$.

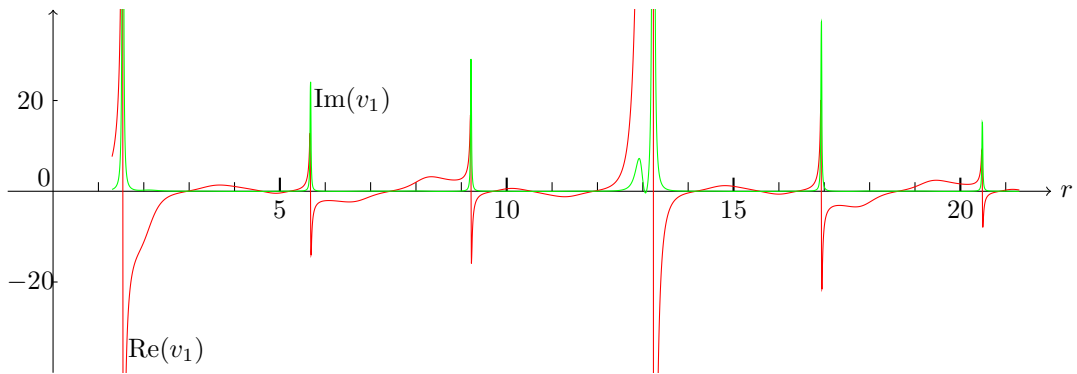


Figure 9: Plot of $v_1(r + 10^{-2}i)$

Although we cannot give a precise description of Figure 8 and Figure 9, we can still make several heuristic observations from the two figures. First, we can safely say that both $v_0(r)$ and $v_1(r)$ have infinity of singularities since some adjacent singularities are almost equidistant. Second, $v_0(r)$ and $v_1(r)$ should be real since the imaginary parts of $v_0(r + 10^{-2}i)$ and $v_1(r + 10^{-2}i)$ are small except near the singularities. Third, $v_1(r_{\text{singular}} + 0_-) > 0$ and $v_1(r_{\text{singular}} + 0_+) < 0$ and the imaginary part of $v_1(r + 0_+i)$ is always positive. Fourth, the singularities of $v_0(r)$ have two frequencies: The class of singularities with $v_0(r_{\text{singular}} + 0_+i) < 0$ have one frequency and the class of singularities with $v_0(r_{\text{singular}} + 0_+i) > 0$ have another frequency. The first two observations should be general for cases deviating from (14). It seems that there is no simple combination of v_0 and v_1 such that the composite variable is smooth for $r \in (0, \infty)$.

6 Conclusion and discussion

This paper numerically studies equation (7), the case 4a of the tt^* -Toda equation. The fine asymptotics of the solutions described by Theorem 1.1 are verified with an accuracy of order 10^{-100} . We enlarge the class of the solutions described by Theorem 1.1 from the Stokes data side and find all the fine asymptotics for the enlarged class of solutions. The associated truncation equations of (7) are crucial for the realization of the high-precision verifications and are indeed useful in the search for the new fine asymptotics. Some preliminary numerical studies are also made to investigate what happens when the fine asymptotics is broken at the $r = 0$ side.

However, the studies in Section 5 are far from complete in investigating the deviation from (14). The first problem is whether we can find two proper dependent variables that are smooth near $r = \infty$. It can be shown that the singularity of $\frac{1}{v_0(r)}$ coincides with $v_1(r)$, differing only in amplitude. But this does not help much in determining what are the proper variables. Without smooth variables it will be almost impossible to talk about the asymptotics near $r = \infty$. The second problem is to find out the $r = \infty$ asymptotics of (65) beyond $v_0(r) \xrightarrow{r \rightarrow \infty} \pm 1$, $v_1(r) \xrightarrow{r \rightarrow \infty} \pm 1$ ¹. Perhaps the best way to explain this is to look at the similar but opposite case. In Conjecture 4.1, the problem starts from the $r = \infty$ side and we see no classification near $r = \infty$ until the solutions evolve to the $r = 0$ side where different types of asymptotics near $r = 0$ are observed. Section 5 starts from the $r = 0$ side and we see no classification near $r = 0$ for the cases parameterized by points in the triangle. We expect the behavior of these solutions to separate near $r = \infty$ and provide a natural classification of the $r = \infty$ asymptotics of (65).

Acknowledgement

Part of this work was done while Y. Li was visiting the Department of Mathematical Sciences of IUPUI. Y. Li would like to thank A. Its for his hospitality and the suggestion of verifying their Corollary 8.3 in [7]. The work is partly supported by NSFC(12235007) and Science and Technology Commission of Shanghai Municipality (No. 22DZ2229014).

References

- [1] Cecotti S. and Vafa C., Topological-anti-topological fusion, *Nucl. Phys. B* 367(1991), 359-461.
- [2] Cecotti S. and Vafa C., Exact results for supersymmetric σ models, *Phys. Rev. Lett.* 68(1992), 903-906.
- [3] Cecotti S. and Vafa C., On classification of $N = 2$ supersymmetric theories, *Commun. Math. Phys.* 158(1993), 569-644.
- [4] Dubrovin B., Geometry and integrability of topological-antitopological fusion, *Commun. Math. Phys.* 152(1993), 539-564.
- [5] Martin A. Guest, Alexander R. Its and Chang-Shou Lin, Isomonodromy aspects of the tt^* equations of Cecotti and Vafa I. Stokes data, *Int. Math. Res. Notices* Vol. 2015, No.22, 11745-11784.

¹Obviously, $v_0(r) \xrightarrow{r \rightarrow \infty} 1$, $v_1(r) \xrightarrow{r \rightarrow \infty} 1$ is equivalent to $w_0(r) \xrightarrow{r \rightarrow \infty} 0$, $w_1(r) \xrightarrow{r \rightarrow \infty} 0$. From the symmetry of (65), the solutions of $v_0(r) \xrightarrow{r \rightarrow \infty} -1$, $v_1(r) \xrightarrow{r \rightarrow \infty} -1$ can be obtained from the one of $v_0(r) \xrightarrow{r \rightarrow \infty} 1$, $v_1(r) \xrightarrow{r \rightarrow \infty} 1$ by a substitution $v_0 \rightarrow -v_0$, $v_1 \rightarrow -v_1$.

- [6] Martin A. Guest, Alexander R. Its and Chang-Shou Lin, Isomonodromy aspects of the tt^* equations of Cecotti and Vafa II. Riemann-Hilbert problem, *Commun. Math. Phys.* 336(2015), 337-380.
- [7] Martin A. Guest, Alexander R. Its and Chang-Shou Lin, Isomonodromy aspects of the tt^* equations of Cecotti and Vafa III: Iwasawa factorization and asymptotics. *Commun. Math. Phys.* 374(2020), 923-973.
- [8] Martin A. Guest, Alexander R. Its and Chang-Shou Lin, The tt^* -Toda equations of A_n type. preprint(arXiv:2302.04597v2).
- [9] Martin A. Guest and Chang-Shou Lin, Nonlinear PDE aspects of the tt^* equations of Cecotti and Vafa, *J. reine angew. Math.* 689(2014), 1-32.
- [10] Mochizuki T., Harmonic bundles and Toda lattices with opposite sign, preprint(arXiv:1301.1718).
- [11] Mochizuki T., Harmonic bundles and Toda lattices with opposite sign II, *Commun. Math. Phys.* 328(2014), 1159-1198.

YUQI Li

School of Mathematical Sciences, Key Laboratory of MEA & Shanghai Key Laboratory of PMMP

East China Normal University

Shanghai 200241

People's Republic of China

E-mail: yqli@sei.ecnu.edu.cn